Available online at www.sciencedirect.com

ScienceDirect

Geochimica et Cosmochimica Acta 328 (2022) 221–241

Geochimica et Cosmochimica Acta

www.elsevier.com/locate/gca

Magma oceans, iron and chromium redox, and the origin of comparatively oxidized planetary mantles

M.M. Hirschmann

Dept. of Earth and Environmental Sciences, University of Minnesota, Minneapolis, MN 55455, USA

Received 13 October 2021; accepted in revised form 6 April 2022; Available online 4 May 2022

Abstract

The mantles of both Earth and Mars are more oxidized than would be expected based on low pressure equilibration of molten silicate and alloy during their magma ocean stages. High pressure silicate-alloy equilibration in a magma ocean can produce appreciable ferric iron in the silicate, leading to comparatively oxidized near surface conditions and overlying atmospheres. Upon crystallization, this may feasibly be sufficient to account for oxygen fugacities prevailing in basalt source regions of Earth and Mars. Experiments and first principles studies affirm that Fe^{3+} is stabilized at high pressure, but to date there has been no model that accounts accurately for the combined effects of melt composition, temperature, pressure, and oxygen fugacity on magma ocean Fe^{3+}/Fe^{T}. We calibrate a new model for Fe^{3+}/Fe^{T} as a function of temperature, pressure, melt composition, and f_{O2} which reproduces Fe^{3+}/Fe^{T} for experimental peridotite liquids and which incorporates differences in FeO and Fe_2O_3 liquid heat capacities into a potentially realistic temperature function. For the effects of pressure, two versions of the model are implemented based on recent equations of state (EOS), though only the EOS of Deng et al. (2020) is applicable to pressures relevant to metal-silicate equilibration in a deep terrestrial magma ocean. For Earth, metal-silicate equilibration at 28–53 GPa, 2300–4100 K, and f_{O2} set by plausible mantle and core compositions produces Fe^{3+}/Fe^{T} between 0.034 and 0.10, with variation mostly owing to differences in assumed temperatures. For Mars, different proposed mantle compositions produce Fe^{3+}/Fe^{T} ratios that range from 0.026 for FeO* of 13.5 wt.% up to 0.038 for FeO* of 18.1 wt.%.

Although significant Fe^{3+} may be present in magma oceans owing to high pressure equilibration with alloy, the budget of Fe_2O_3 in crystallized mantles is expected to be modified from that in the molten state. An important additional factor is the influence of Cr, which is Cr^{2+} in molten silicate equilibrated with alloy and Cr^{3+} in terrestrial upper mantles. Production of Cr^{3+} and Fe^{2+} by reaction with Cr^{2+} and Fe^{3+} during crystallization can destroy much of the Fe_2O_3 present during the magma ocean stage. Considering the stability of Cr^{2+} in olivine and the temperature-dependent partitioning of Cr^{3+} between mantle silicates, we construct an empirical model for the fraction of Cr that is Cr_2O_3 in solid spinel peridotite as a function of temperature and f_{O2}. For Earth, at least 0.35 wt.% Fe_2O_3 is destroyed by oxidation of magma ocean CrO and for Mars, more than 0.55 wt.% Fe_2O_3 should be destroyed. Consequently, either the terrestrial and martian magma oceans were significantly more enriched in Fe_2O_3 than their present-day upper mantles or other processes contributed to oxidation of the latter. Overenrichment of Fe_2O_3 in the magma oceans is plausible only if terrestrial metal-silicate equilibration occurred above 3300 K and if the martian mantle contains >17 wt.% FeO*. Subsolidus disproportionation of ferrous iron may have contributed to the present-day redox state of the Earth's mantle, and late accretion of chondrite-like material and hydrogen degassing also likely affected the solidified mantles of both Earth and Mars.
© 2022 Elsevier Ltd. All rights reserved.

Keywords: Magma ocean; Iron redox; Chromium; Earth; Mars

E-mail address: mmh@umn.edu

https://doi.org/10.1016/j.gca.2022.04.005
0016-7037/© 2022 Elsevier Ltd. All rights reserved.

1. INTRODUCTION

Planetary mantles originate during the magma ocean stage of differentiation, as metallic alloy segregates from molten silicate, which then crystallizes. Reaction with Fe-rich alloy imposes reducing conditions on the molten silicate, but the mantles of both Earth and Mars are more oxidized than would be expected based on low pressure silicate-alloy equilibration (Frost et al., 2008). These more oxidized conditions affect geochemical and geodynamical evolution during the magma ocean phase and subsequently, including early mantle outgassing and retention of volatiles in the nascent mantle, and have ongoing influence on climate and the potential for prebiotic chemistry (Hirschmann, 2012; Armstrong et al., 2019; Deng et al., 2020; Sossi et al., 2020).

Reaction between core-destined alloy and molten silicate fixes the oxygen fugacity according to the reaction

$$\underset{\text{molten alloy}}{\text{Fe}} + 1/2\ \text{O}_2 \Longleftrightarrow \underset{\text{molten silicate}}{\text{FeO}} \quad (1)$$

For a terrestrial magma ocean with ~8 wt.% FeO, this reaction sets the f_{O2} to approximately two orders of magnitude below the iron-wüstite (IW) reference buffer (Frost et al., 2008), defined by the coexistence of pure crystalline Fe and $Fe_{1-y}O$ (Hirschmann, 2021). In contrast, Earth's upper mantle is 3–5 orders of magnitude more oxidizing than IW and has been so at least since the early Hadean (Delano, 2001; Canil, 2002; Trail et al., 2011). The high comparative oxygen fugacity of the terrestrial upper mantle is manifested by an appreciable concentration of Fe^{3+}. Based on xenoliths, basalts, and thermodynamic calculations, the proportion of Fe in Earth's upper mantle that is ferric, denoted as Fe^{3+}/Fe^{T}, is between 0.02 and 0.06 (O'Neill et al., 1993; Canil et al., 1994; Canil and Oneill, 1996; Woodland et al., 2006; Cottrell and Kelley, 2011; Gaetani, 2016; Sossi et al., 2020; Davis and Cottrell, 2021), which translates to 0.16–0.48 wt.% Fe_2O_3 for mantle with 8 wt.% FeO* (McDonough and Sun, 1995) (where FeO* signifies all Fe expressed as FeO). Mars also has an offset between the f_{O2} expected from magma ocean-core equilibration and the f_{O2} recorded by basalts, though it is less pronounced than for Earth. The conditions of martian core formation are typically estimated to be at IW−2 to IW−1.5, though they depend on the FeO content of the martian mantle, for which there is some uncertainty (13.5-18.1 wt.%; Taylor, 2013; Khan et al., 2018; Yoshizaki and McDonough, 2020). Recent estimates based on geophysical constraints from the InSight mission favor FeO* concentrations at the low end of this span (Khan et al., 2022). In contrast, the most reduced martian basalts record f_{O2} near IW (Herd, 2008; Schmidt et al., 2013; Nicklas et al., 2021). Many martian basalts are yet more oxidized, ranging up to IW+5 (Schmidt et al., 2013; Santos et al., 2015), and plausibly may represent either more enriched mantle domains or the effects of processes in the crust (Herd, 2008; Nicklas et al., 2021).

A significant process producing oxidized mantle is disproportionation of ferrous iron to metallic and ferric iron at high pressure. Iron disproportionation was originally considered to be driven by crystallization of Fe^{3+}-rich silicates or oxides at high pressure (Mao, 1974; Frost et al., 2004), but could also occur directly in the magma ocean, owing to stabilization of Fe^{3+} in high pressure silicate melts (Hirschmann, 2012; Zhang et al., 2017; Armstrong et al., 2019; Deng et al., 2020). The distinction is important, as the two imply different mechanisms and timing for the oxidative transition. Disproportionation associated with crystallization requires that coevally formed alloy be transported to the core by an additional later process. A separate episode of core segregation is not required if disproportionation is driven by magma-alloy equilibration. The latter may also impose relatively oxidized conditions at the surface of the magma ocean, owing to the pressure dependence of ferric-ferrous equilibrium in the melt (Hirschmann, 2012; Sossi et al., 2020), whereas the former does not transmit more oxidizing conditions to the surface until convective overturn of the solidified mantle brings the oxidized residue into the upper mantle. Thus, the redox state during the main stage of magma ocean evolution has important effects on how a magma ocean retains volatiles or expels them to the overlying atmosphere (Hirschmann, 2012; Armstrong et al., 2019; Deng et al., 2020; Sossi et al., 2020). The different disproportionation processes are not mutually exclusive, as Fe^{3+} could be stable at magmatic conditions and be further enhanced during crystallization.

In addition to iron disproportionation, several other processes may play important roles. One of these is hydrogen escape (Hunten, 1973; Dreibus and Wanke, 1987; Hamano et al., 2013; Sharp et al., 2013; Sharp, 2017; Pahlevan et al., 2019) though on the basis of D/H isotopes, the extent of the latter was limited if the source of hydrogen delivered to Earth was similar to chondrites (Pahlevan et al., 2019). Another is reaction with material added during post-magma ocean late-accretion (Pahlevan et al., 2019; Nicklas et al., 2021). Also, fractional crystallization during magma ocean crystallization can create oxidized domains (Schaefer and Elkins-Tanton, 2018), though it shouldn't affect whole-mantle redox mass balance. Finally, secular evolution through subsequent tectonic and magmatic history may have modified the terrestrial mantle (Aulbach et al., 2019; Nicklas et al., 2019), and plausibly the martian mantle also. In the case of Earth, this is thought to be a secondary effect, modifying conditions that were already comparatively oxidized by the early Hadean (Delano, 2001; Canil, 2002; Trail et al., 2011).

Stabilization of appreciable Fe^{3+} in alloy-saturated magma at high pressure was presented initially as a speculation (Hirschmann, 2012), but was not confirmed by a preliminary experimental study to 7 GPa (Zhang et al., 2017). Later, experiments up to 23 GPa (Armstrong et al., 2019) and first principles calculations (Deng et al., 2020) showed that Fe^{3+} in alloy-saturated silicate liquids does increase with pressure. Recent investigations at low pressure have provided the first experimental constraints on the relationship between f_{O2} and the stability of Fe^{3+} in peridotitic melts (Sossi et al., 2020), as compared to less magnesian analogs on which earlier work relied. Together, these indicate that magma oceans equilibrated with iron alloy at high

pressure can have small but significant ferric iron concentrations. However, the new studies are not wholly consistent with one another and do not resolve fundamental questions, including whether the amount of Fe^{3+} present during the magma ocean stage was sufficient to account for the present-day redox inventory of Earth's mantle and whether the modest pressures of alloy-silicate equilibration during core separation on Mars stabilized sufficient Fe^{3+} to account for the comparatively oxidized state of the martian mantle sampled by basalts.

An important additional factor, to our knowledge not previously considered, is the role of chromium. Whereas nearly all Cr in silicate liquid is Cr^{2+}under the conditions relevant to core-mantle equilibration (Corgne et al., 2008; Mann et al., 2009; Siebert et al., 2011; Steenstra et al., 2020), most of it is Cr^{3+} in solidified upper mantle peridotite (Li et al., 1995; Witt-Eickschen and O'Neill, 2005). During mantle crystallization, Cr is oxidized in an intervalence exchange reaction with iron

$$\underset{\text{magma}}{Fe_2O_3} + 2\,\underset{\text{magma}}{CrO} \Longleftrightarrow \underset{\text{peridotite}}{Cr_2O_3} + 2\,\underset{\text{peridotite}}{FeO} \quad (2)$$

thereby diminishing the Fe^{3+} available to solid mantle assemblages. This has the effect of producing a more reduced solid mantle than would result from solidification of an iron-bearing Cr-free system. The effect of Cr is important even though it is far less abundant than Fe in peridotite because a much larger fraction of the Cr changes valence.

Here we investigate quantitatively the effects of iron disproportionation in a magma ocean and of Cr-Fe intervalence transfer on the redox transformation of Earth and Mars from the conditions imposed by core formation to those prevailing in their basalt source regions. The chief aim is to evaluate whether these processes together can account for significant ferric iron in the upper mantles of Earth and Mars. An associated aim is to highlight those places where quantitative evaluation is limited by current understanding of fundamental thermodynamic properties of ferric and ferrous iron at magma ocean conditions.

2. ALLOY-SILICATE EQUILIBRATION AND MAGMA OCEAN f_{O2}

The oxygen fugacity set by equilibration between molten silicate and core-destined alloy depends on the compositions of the liquids and on the temperature and pressure of equilibration. Numerous studies have sought to characterize the conditions of core formation on Earth, Moon, and Mars, chiefly by characterizing the effects of temperature and pressure on partitioning of siderophile elements (e.g., Li and Agee, 1996; Righter and Drake, 1996; Gessmann and Rubie, 2000; Gessmann et al., 2001; Li and Agee, 2001; Siebert et al., 2012). However, the history of metal-silicate reaction during planetary accretion and differentiation is dynamic, evolving as a planet grows (Rubie et al., 2011; Siebert et al., 2013) and punctuated by giant impacts, which may impose transient high temperature episodes of core segregation (Lock and Stewart, 2017). Further, the conditions of metal-silicate equilibration are controlled in part by kinetic parameters and dynamical factors such as the length-scales of core-destined blobs or droplets and the effective time scales of magma ocean homogenization (Deguen et al., 2014). Consequently, there is no unique set of compositions and conditions at which a planet's core and molten mantle equilibrate. Any estimated set of pressure and temperature conditions should be understood as a characteristic average of processes that happened over a range of conditions and such averages may have different significance, depending on whether the chief parameter of interest is the masses of siderophile elements removed to the core or the conditions prevailing in the magma ocean when core-mantle separation terminated. The former should remember the integrated history of core-mantle equilibration conditions, whereas the latter may depend chiefly on the conditions of last separation of metal from a convecting and well-mixed molten mantle. More advanced treatments may reconcile these differences by forward modeling the history of metal-silicate separation during accretion and differentiation (Rubie et al., 2011; Siebert et al., 2013), though these also depend on assumptions about the accretion history and the details of metal-silicate equilibration. Such models also incorporate heterogeneous accretion, such that the arriving compositions of molten silicate and core-destined alloy evolve through the differentiation process. For present purposes, it is the composition of the silicate and alloy that separate at the termination of core segregation that determine the redox characteristics of the net material destined to form the earliest solidified mantle. In most cases, this should be quite similar to the composition of the bulk silicate mantle that can be estimated from present-day observations of rocks and geophysical characteristics. The complementary alloy composition is partly model-dependent, but fortunately, except as noted below, has only a second-order effect on calculated oxygen fugacities

To explore the effects of silicate-alloy equilibration conditions on the oxygen fugacity imposed on a magma ocean, we consider a representative range of estimates of nominal core-forming conditions, silicate, and alloy compositions (Table 1). Although most of these are derived from siderophile element abundances, and therefore may not describe well the temperatures and pressures of final silicate-alloy equilibration, the estimates allow exploration how the temperatures and pressures of alloy separation affect magma ocean f_{O2} and Fe^{3+}/Fe^{T}. For Earth, estimated pressures and temperatures vary widely (28–53 GPa, 2250–4100 K; see sources in Table 1). We take the silicate composition, 8 wt.% FeO*, as that of the bulk silicate Earth (McDonough and Sun, 1995) and examine a range of proposed core compositions (Table 1). For Mars, estimates of core-forming conditions lie in a narrow range (14 ± 1 GPa, 2200 ± 200 K; Rai and van Westrenen, 2013; Righter et al., 2015; Righter et al., 2020), but estimates of mantle (13.5–18.1 wt.% FeO*) and core compositions are diverse. Although not of direct relevance to the main aim of this paper, for completeness we also include estimates applicable to the lunar magma ocean, with core segregation conditions of 3.5–4.8 GPa, 2200–3150 K, and 7.6–12 wt.% FeO* in the magma ocean (Table 1).

Table 1
Magma ocean compositions and conditions.

Silicate				Alloy		Conditions				
FeO* wt.%	Cr_2O_3 wt.%	X_{FeO}	a_{FeO}	X_{Fe}	a_{Fe}	T (K)	P (GPa)	ΔIW*	ΔIW	log f_{O2}
Mars										
14.7[a]	0.88[a]	0.108[a]	0.167	0.681[a]	1.011[†]	2200[r]	14[r]	−1.56	−1.48	−3.75
17.9[b]	0.76[b]	0.133[b]	0.206	0.701[b]	0.801	2200[r]	14[r]	−1.18	−1.10	−3.37
18.1[c]	0.73[c]	0.137[c]	0.213	*0.632*[c]	0.851	2200[r]	14[r]	−1.20	−1.12	−3.39
15.9[d]	0.65[d]	0.119[d]	0.185	0.862[d]	0.865	2200[r]	14[r]	−1.34	−1.26	−3.53
17.2[e]	0.68[e]	0.127[e]	0.197	0.754[e]	0.803	2200[r]	14[r]	−1.22	−1.14	−3.41
17.0[f]	–	0.126[f]	0.195	0.580[f]	0.755	2200[r]	14[r]	−1.17	−1.09	−3.36
16.0[g]	–	0.121[g]	0.188	*0.770*[g]	0.827	2200[r]	14[r]	−1.29	−1.21	−3.48
13.5[g]	–	0.100[g]	0.155	*0.807*[g]	0.840	2200[r]	14[r]	−1.47	−1.39	−3.65
13.7[h]	–	0.099	0.154	*0.637*[h]	0.780	2200[r]	14[r]	−1.41	−1.33	−3.60
Moon										
10.9[i]	0.61[i]	0.079[i]	0.122	0.886[l]	0.877	2200[s]	3.5[s]	−1.71	−1.89	−6.79
10.9[i]	0.61[i]	0.079[i]	0.122	0.734[m]	0.565	2200[s]	3.5[s]	−1.33	−1.51	−6.41
10.9[i]	0.61[i]	0.079[i]	0.122	0.856[n]	0.842	2200[s]	3.5[s]	−1.68	−1.86	−6.76
7.6[j]	0.5[j]	0.054[j]	0.083	0.886[m]	0.877	2250[m]	4.8[m]	−2.05	−2.21	−6.53
7.6[j]	0.5[j]	0.054[j]	0.083	0.734[m]	0.565	2250[m]	4.8[m]	−1.66	−1.83	−6.15
7.6[j]	0.5[j]	0.054[j]	0.083	0.856[n]	0.842	2250[m]	4.8[m]	−2.01	−2.18	−6.50
12[k]	0.3[k]	0.089[k]	0.137	0.886[m]	0.877	3150[m]	4.8[m]	−1.61	−2.09	−3.35
12[k]	0.3[k]	0.089[k]	0.137	0.734[m]	0.565	3150[m]	4.8[m]	−1.23	−1.71	−2.96
12[k]	0.3[k]	0.089[k]	0.137	0.856[n]	0.842	3150[m]	4.8[m]	−1.57	−2.06	−3.31
Earth										
8.0[l]	0.38[l]	0.056[l]	0.087	0.792[o]	0.791	2250[t]	28[t]	−1.91	−1.59	−0.47
8.0[l]	0.38[l]	0.056[l]	0.087	0.727[p]	0.637	2250[t]	28[t]	−1.72	−1.40	−0.28
8.0[l]	0.38[l]	0.056[l]	0.087	0.788[q]	0.866	2250[t]	28[t]	−1.99	−1.67	−0.55
8.0[l]	0.38[l]	0.056[l]	0.087	0.792[o]	0.791	4100[u]	40[u]	−1.91	−2.49	2.49
8.0[l]	0.38[l]	0.056[l]	0.087	0.727[p]	0.676	4100[u]	40[u]	−1.78	−2.36	2.63
8.0[l]	0.38[l]	0.056[l]	0.087	0.788[q]	0.830	4100[u]	40[u]	−1.95	−2.54	2.45
8.0[l]	0.38[l]	0.056[l]	0.087	0.792[o]	0.791	3250[v]	50[v]	−1.91	−1.93	4.00
8.0[l]	0.38[l]	0.056[l]	0.087	0.727[p]	0.663	3250[v]	50[v]	−1.76	−1.78	4.16
8.0[l]	0.38[l]	0.056[l]	0.087	0.788[q]	0.841	3250[v]	50[v]	−1.97	−1.99	3.95
8.0[l]	0.38[l]	0.056[l]	0.087	0.792[o]	0.791	3600[w]	53[w]	−1.91	−2.12	4.25
8.0[l]	0.38[l]	0.056[l]	0.087	0.727[p]	0.669	3600[w]	53[w]	−1.77	−1.98	4.40
8.0[l]	0.38[l]	0.056[l]	0.087	0.788[q]	0.836	3600[w]	53[w]	−1.96	−2.17	4.20
8.0[l]	0.38[l]	0.056[l]	0.087	0.792[o]	0.791	3300[w]	35[x]	−1.91	−2.10	1.75
8.0[l]	0.38[l]	0.056[l]	0.087	0.727[p]	0.664	3300[x]	35[x]	−1.76	−1.94	1.91
8.0[l]	0.38[l]	0.056[l]	0.087	0.788[q]	0.841	3300[x]	35[x]	−1.97	−2.15	1.70

ΔIW* is the log fO_2 relative to conditions buffered by pure liquid Fe and FeO; ΔIW is relative to pure crystalline Fe and wüstite. [†]An activity >1 indicates that the Ma (2001) solution model predicts that the oxygen-rich core composition favored by Yoshizaki and McDonough (2020) is inside a miscibility gap at the specified temperature. Martian core compositions with X_{Fe} in italics indicates publications that did not specify a Ni concentration. In these cases, we assume Ni/(Ni + Fe) = 0.085, similar to other martian core estimates.
(a) Yoshizaki and McDonough (2020), (b) Wänke and Dreibus (1994), (c) Taylor (2013), (d) Morgan and Anders (1979), (e) Lodders and Fegley (1997), (f) Khan and Connolly (2008), (g) Liebske and Khan (2019), (h) Khan et al. (2022), (i) Taylor (1982), (j) Longhi (2006), (k) Snyder et al. (1992), (l) McDonough and Sun (1995), (m) Steenstra et al. (2017), (n) Righter et al. (2017), (o) McDonough (2003), (p) Litasov and Shatskiy (2016), (q) Badro et al. (2014), (r) Righter et al. (2015), (s) Righter and Drake (1996), (t) Li and Agee (1996), (u) Gessmann et al. (2001), (v) Li and Agee (2001), (w) Siebert et al. (2012), (x) Gessmann and Rubie (2001).

The coexistence of FeO-bearing silicate melt and molten Fe-rich alloy allows calculation of oxygen fugacity through reaction (1). It is common practice to consider this reference reaction as being equivalent to the "iron wüstite" (IW) buffer (e.g., Li and Agee, 1996; Siebert et al., 2012; Chi et al., 2014). However, some care should taken in the definition of "iron wüstite". We term reaction (1) "IW*" and it represents equilibrium between two pure molten phases, and we report logarithmic deviations of f_{O2} from it as ΔIW*. For IW*, the standard states for which unit activity applies are liquid Fe and liquid FeO, whereas representations of the high pressure IW buffer (Campbell et al., 2009; Fischer et al., 2011; Hirschmann, 2021) refer to crystalline standard states:

$$\underset{solid\ alloy}{Fe} + 1/2\,O_2 \Longleftrightarrow \underset{solid\ oxide}{FeO\ (IW)} \quad (3)$$

IW* and IW impart somewhat different oxygen fugacities, with greater differences further from the fusion temperatures of pure Fe and FeO, as quantified below.

Calculation of ΔIW* for a given silicate/alloy pair at the temperature and pressure of interest requires evaluation of the activity coefficients, $\gamma_{component}^{phase}$, of Fe and FeO:

$$a_{Fe}^{alloy} = \gamma_{Fe}^{alloy} X_{Fe}^{alloy}; a_{FeO}^{silicate} = \gamma_{FeO}^{silicate} X_{FeO}^{silicate} \quad (4a, 4b)$$

Values of γ_{Fe}^{alloy} are calculated with the methods of Ma (2001), using the calculator (http://norris.org.au/expet/metalact) supplied by Norris and Wood (2017) (Table 1). The value of $\gamma_{FeO}^{silicate}$ in silicate melts is derived by examination of high pressure experiments in which ultramafic melts coexist with ferropericlase (fp), following Rubie et al. (2004). Alternative experimental values of $\gamma_{FeO}^{silicate}$ come from gas mixing experiments in which silicate melts were equilibrated with metallic Fe at known f_{O2} (e.g., Doyle, 1988; O'Neill and Eggins, 2002; Holzheid and Grove, 2005), but those from ferropericlase-melt experiments are preferred because they give constraints at temperatures, pressures, and melt compositions that are more applicable to core-segregation in magma oceans.

For experimental pairs of coexisting ferropericlase and silicate melt at known temperature and pressure, the equilibrium

$$\underset{fp}{FeO} \Longleftrightarrow \underset{liquid}{FeO} \quad (5)$$

gives the activity of FeO in the liquid according to

$$a_{FeO}^{liq} = a_{FeO}^{fp} \exp\left(-\Delta G_{FeO}^{fusion}/RT\right) \quad (6)$$

Therefore

$$\gamma_{FeO}^{silicate} = \frac{a_{FeO}^{fp}}{X_{FeO}^{silicate}} \exp\left(-\Delta G_{FeO}^{fusion}/RT\right) \quad (7)$$

in which a_{FeO}^{fp} is calculated from the composition of ferropericlase and the non-ideal mixing model of Frost (2003), $\gamma_{FeO}^{silicate}$ is calculated on a 1-cation oxide basis and ΔG_{FeO}^{fusion} is evaluated from the thermodynamic models of Komabayashi (2014).

Compiled experimental ferropericlase-silicate pairs (Fig. 1) span 2–33 GPa and 2023–2900 K (Table S1). For melts with $X_{FeO}^{silicate} > 0.1$, these produce $\gamma_{FeO}^{silicate}$ values in the range of 1.55 ± 0.19 ($n = 16$), with no evident dependence on temperature, pressure, or melt composition. Those with $X_{FeO}^{silicate} < 0.1$ indicate higher $\gamma_{FeO}^{silicate}$. This apparent non-Henrian behavior is not seemingly owing to the effects of temperature, pressure, or concentrations of major melt species (SiO_2, MgO), as these are not systematically different between the high and low $X_{FeO}^{silicate}$ experiments. We suspect that the high $\gamma_{FeO}^{silicate}$ values at low $X_{FeO}^{silicate}$ are artifacts of application of the ferropericlase activity-composition model of Frost (2003) to low-FeO oxides, as this model was calibrated only from more FeO-rich experiments. Possibly asymmetric mixing effects in low FeO ferropericlase are not captured by this symmetric solution model. Consequently, we apply $\gamma_{FeO}^{silicate}$ of 1.55 for all the proposed magma ocean compositions that we consider. If the greater values of $\gamma_{FeO}^{silicate}$ at low $X_{FeO}^{silicate}$ evident in Fig. 1 are accurate, then calculated values of ΔIW* and ΔIW for the less FeO-rich, such as that of Earth ($X_{FeO}^{silicate} = 0.056$; Table 1) or the FeO-poor lunar mantle composition of Longhi (2006) ($X_{FeO}^{silicate} = 0.054$), are about 0.2 log units too reduced.

Using the above thermodynamic models, calculated values of ΔIW* for magma ocean-alloy equilibration depend chiefly on silicate FeO* concentrations, as has been long known (e.g., Frost et al., 2008). For Earth, values of ΔIW* range from −2 to −1.7 (Table 1) and depend on assumed molten alloy compositions, with more oxidized values corresponding to higher Si and C and lower O and S concentrations. Calculated values of ΔIW* for Mars and the Moon span −1.6 to −1.2 and −2.1 to −1.2 respectively, and vary largely because of variable estimates of FeO* concentrations in their mantles (Table 1). The more oxidized IW* values for the Moon are based on C-rich core compositions advocated by Steenstra et al. (2017).

The absolute f_{O2} of IW* as a function of temperature and pressure can be evaluated from Eq. (1), given by

$$\log f_{O_2} = \frac{2}{\ln(10)}\left(G_{FeO}^{liq} - G_{Fe}^{liq} - 1/2 G_{O_2}\right) \quad (8)$$

calculating values of G_{FeO}^{liq} and G_{FeO}^{liq} from Komabayashi (2014) and G_{O_2} from JANAF (Chase, 1998). This allows translation of the ΔIW* values for each set of magma ocean-alloy equilibration conditions depicted in Fig. 2A to values of f_{O2} (Table 1), which can be used to calculate magmatic Fe^{3+}/Fe^{T}.

It is also of interest to calculate the f_{O2} imparted by silicate-alloy equilibration relative to the solid IW buffer. The oxygen fugacities calculated from Eq. (8) can be translated to values of ΔIW based on the iron-wüstite parameterization given by Hirschmann (2021). IW crosses from more reduced than IW* to more oxidized at temperatures near the melting points of FeO and so resulting values of ΔIW for magma ocean-alloy equilibration conditions have a greater spread than those relative to ΔIW*, with the more relatively reduced values corresponding to higher temperature estimates. For Earth, Mars and the Moon, calculated values of IW range from −2.5 to −1.4, −1.5 to −1.1, and −2.2 to −1.5, respectively (Fig. 2B). The more reduced ΔIW values for Earth come from high temperature estimates of core formation, conditions at which ΔIW and ΔIW* are more distinct. Likewise, the span for Mars differs little from that based on ΔIW* because the estimated condition of core formation is not too distant from the iron and FeO fusion temperatures.

3. EFFECT OF MELT COMPOSITION, TEMPERATURE, AND PRESSURE ON SILICATE LIQUID FE^{3+}/FE^{T}

For a silicate liquid at specified temperature, pressure, and oxygen fugacity, the ratio of Fe^{3+} and Fe^{2+} can be evaluated from the reaction

$$FeO + 1/4 O_2 = FeO_{1.5} \quad (9)$$

and its associated equilibrium constant

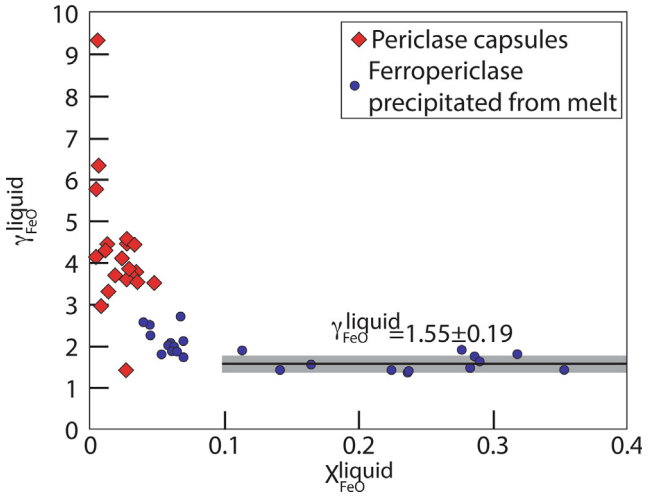

Fig. 1. Values of $\gamma^{silicate}_{FeO}$ calculated from ferropericlase-silicate melt pairs coexisting at 2–33 GPa and 2023–2900 K (Table S1), as described in the text. Data include ferropericlase crystallized from the melt during the experiment and produced by interaction between FeO-bearing melts and MgO capsule material. $\gamma^{silicate}_{FeO}$ for melts with $X^{silicate}_{FeO} > 0.1$ have mean values of 1.55 ± 0.19. Those with $X^{silicate}_{FeO} < 0.1$ have greater values of $\gamma^{silicate}_{FeO}$, but this apparent non-Henrian effect may be an artifact (see text).

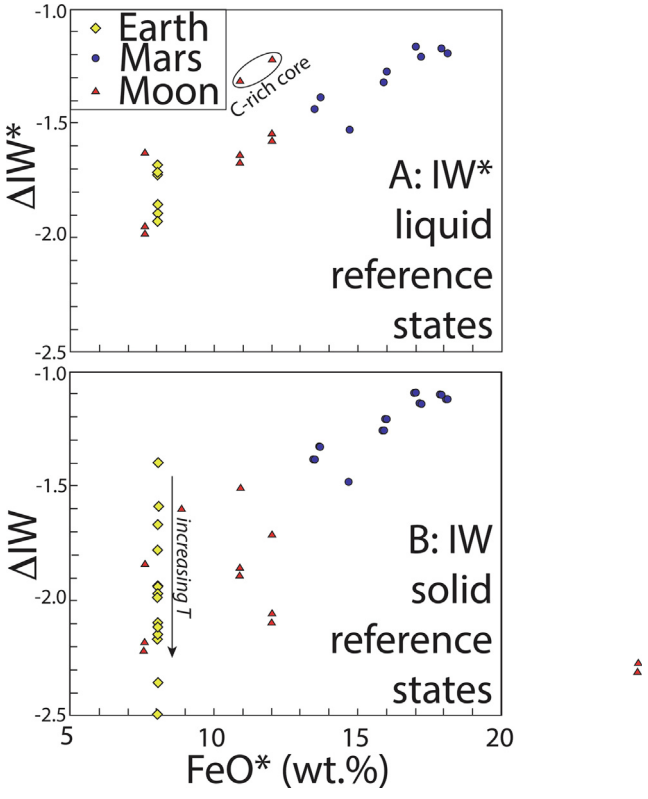

Fig. 2. Values of (A) ΔIW* and (B) ΔIW calculated for magma ocean silicate coexisting with alloy for different estimates of core-forming conditions on Earth, Mars, and the Moon, as described in the text, where ΔIW* and ΔIW are respectively the differences in log f_{O2} from reference buffers defined by coexistence of Fe(liquid) + FeO(liquid) and Fe(solid) + wüstite (solid).

$$\log(K) = \log\left(\frac{a^{melt}_{FeO_{1.5}}}{a^{melt}_{FeO} f_{O_2}^{1/4}}\right) = \frac{\left(\Delta G_{T,P_0} + \int_{T,P_0}^{T,P} \Delta V dP\right)}{RT\ln(10)} \quad (10)$$

$$\log\left(\frac{X^{melt}_{FeO_{1.5}}}{X^{melt}_{FeO}}\right) = 0.25\log f_{O_2} + \frac{-\left(\Delta G_{T,P_0} + \int_{T,P_0}^{T,P} \Delta V dP\right)}{RT\ln(10)} - \log\left(\frac{\gamma^{melt}_{FeO_{1.5}}}{\gamma^{melt}_{FeO}}\right) \quad (11)$$

where $\Delta G_{T,P_0}$ is the free energy of reaction (9) at the reference pressure (100 kPa), ΔV is the change in volume of the reaction at T, and a_i, X_i, and γ_i are the activities, mole fractions, and activity coefficients of the condensed reactants. Non-ideal interactions between ferrous and ferric iron in the melt have been accommodated either by adopting models in which FeO and $FeO_{1.5}$ affect the activity coefficient ratio ($\gamma_{FeO1.5}/\gamma_{FeO}$) (Jayasuriya et al., 2004; Zhang et al., 2017; Deng et al., 2020) or by modifying Eq. (11) to allow the dependence on oxygen fugacity to be an empirical parameter, a,

$$\log\left(\frac{X^{melt}_{FeO_{1.5}}}{X^{melt}_{FeO}}\right) = a\log f_{O2} + \frac{-\left(\Delta G_{T,P_0} + \int_{T,P_0}^{T,P} \Delta V dP\right)}{RT\ln(10)} - \log\left(\frac{\gamma^{melt}_{FeO_{1.5}}}{\gamma^{melt}_{FeO}}\right) \quad (12)$$

(Sack et al., 1980; Kress and Carmichael, 1991; Borisov et al., 2018). Among all these models, no single parameterization reproduces accurately Fe^{3+}/Fe^T variations with melt composition, temperature, pressure, and f_{O2} for conditions applicable to magma oceans. In the following sections, we review previous models and relevant experimental data to examine these dependencies. From these, we develop a revised model for application to magma oceans.

3.1. Effect of melt composition

The recent experiments of Sossi et al. (2020) at 2100 ± 50 K and 100 kPa give the first direct measurements of Fe^{3+}/Fe^T in peridotitic liquids (Fig. 3). Sossi et al. (2020) provided an empirical expression (reduced χ^2_v = 23.2; n = 10) that fits the isothermal variation of Fe^{3+}/Fe^T with f_{O2}, but its applicability at other temperatures is uncertain. Previous thermodynamic models for compositional and temperature variation of Fe^{3+}/Fe^T (Kress and Carmichael, 1991; Jayasuriya et al., 2004; Zhang et al., 2017; Borisov et al., 2018; Deng et al., 2020) were calibrated from less magnesian compositions and so extrapolation to peridotitic melts may not be justified. However, the Borisov et al. (2018) model included experiments designed to isolate the effects of MgO variation on Fe^{3+}/Fe^T and reproduces the experimental values better than the empirical fit (reduced χ^2_v = 4.9). The other earlier models severely underpredict Fe^{3+}/Fe^T in peridotitic melts (Fig. 3).

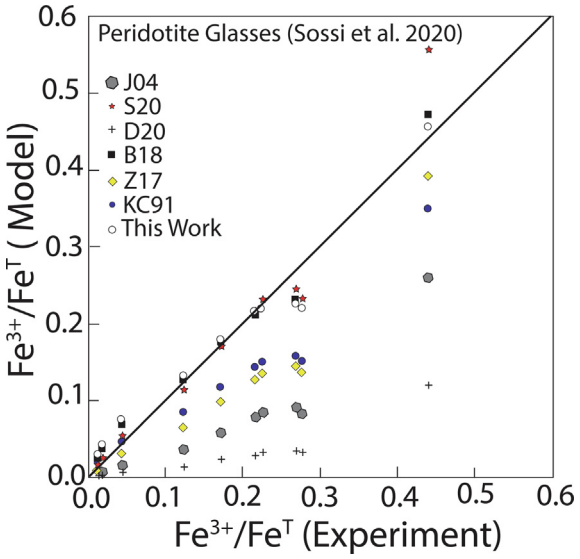

Fig. 3. Fe^{3+}/Fe^T of peridotitic melts from the experiments of Sossi et al. (2020) at 2100 ± 50 K and 100 kPa compared to ratios calculated from models of Kress and Carmichael (1991) (KC91; Eq. (7)), Jayasuriya et al. (2004) (J04; Eq. (14)), Zhang et al. (2017) (Z17), Borisov et al. (2018) (B18), Deng et al. (2020) (D20), Sossi et al. (2020) (S20), and this work (Eq. (21); Table 2). Eq. (21) reproduces these nearly isothermal experiments with accuracy similar to the models of Borisov et al. (2018) and Sossi et al. (2020), but also incorporates improved temperature dependences and accommodates the effects of pressure, as discussed in Sections 3.2–3.4.

3.2. Effect of temperature

The temperature dependence of Fe^{3+}/Fe^T in silicate melts derives chiefly in the change in $\Delta G_{T,P_0}$ (Eq. (12)), though temperature dependences to the activity coefficient ratio can also contribute. Careful attention to the effect of temperature dependence is warranted because the conditions of metal-silicate equilibrium in magma oceans can be several thousand kelvins (Table 1), whereas experimental observations to date are limited to below 2200 K. Accurate assessment of Fe^{3+}/Fe^T in hot deep magma oceans ultimately will require experiments at appropriate temperatures, but at present, reasonable extrapolations must depend on formulations that best capture the relevant influences of temperature.

One approach to estimating parameters for $\Delta G_{T,P_0}$ is to extract it from the properties from simple oxide FeO and $FeO_{1.5}$ liquid (Jayasuriya et al., 2004; Eq. (10) and "ΔG (1)") (Deng et al., 2020; Sossi et al., 2020). This strategy, however, has limitations because constraints on the properties of Fe_2O_3 liquid are poor. Crystalline Fe_2O_3 decomposes to magnetite plus gas at 1730 K (Wriedt, 1991), and therefore neither the fusion temperature, enthalpy, nor heat capacity of Fe_2O_3 liquid have been measured experimentally. Further, the thermodynamic properties of FeO liquid tabulated in JANAF (Chase, 1998), employed in thermodynamic models of reaction (9) by Deng et al. (2020) and Sossi et al. (2020) (and also indirectly in the value of "ΔG(1)" derived by Jayasuriya et al., 2004), are known to be erro-

neous (Hirschmann, 2021). Properties of FeO(l) and Fe_2O_3(l) from the metallurgical literature (Sundman, 1991; Kowalski and Spencer, 1995; Hidayat et al., 2015), derived from modeling liquidus relations in the system Fe-O, do not depend on JANAF and are believed to have accurate estimates of the free energy of FeO liquid (Komabayashi, 2014; Hirschmann, 2021), but for Fe_2O_3(l) their accuracy is poorly established, because direct thermochemical data for Fe_2O_3(l) are not available and because the models are not constrained from phase equilibria data beyond liquids only slightly more O-rich than Fe_3O_4.

$\Delta G_{T,P_0}$ can also be evaluated from homogeneous equilibrium between ferrous and ferric iron in silicate liquids (Sack et al., 1980; Kress and Carmichael, 1991; Zhang et al., 2017; Borisov et al., 2018). This may produce accurate partial molar properties of FeO and Fe_2O_3 that account for bonding and coordination of ferrous and ferric iron cations in silicate liquids. Similar strategies were shown to be successful for deriving heat capacities, volumes, and compressibilities of magmatic liquids (Kress and Carmichael, 1991; Lange and Navrotsky, 1992). In practice, such constraints come from liquids of diverse composition and at variable oxygen fugacities, and so values of delta $\Delta G_{T,P_0}$ are extracted by simultaneous regression with melt mixing parameters (Sack et al., 1980; Kress and Carmichael, 1991; Jayasuriya et al., 2004; Borisov et al., 2018).

A key consideration for extrapolation to high temperature is the nature of the $\Delta G_{T,P_0}$ function employed. Because most available data span a relatively limited temperature range (1500–1900 K), several previous studies (Jayasuriya et al., 2004; Zhang et al., 2017; Borisov et al., 2018) adopt a simple parameterization with a reciprocal temperature dependence

$$\frac{\Delta G_{T,P_0}}{RT} = a + b/T \tag{13}$$

Such functions predict that Fe^{3+}/Fe^T will asymptotically approach a constant value at high temperature (Fig. 4). A more complete representation is given by

$$\Delta G_{T,P_0} = \Delta H + \Delta C_p(T - T_R) - T\left(\Delta S + \Delta C_p ln\frac{T}{T_R}\right) \tag{14}$$

where $\Delta C_p = C_P^{FeO_{1.5}} - C_P^{FeO} - 0.25C_P^{O_2}$ and T_R is a reference temperature. Combining values of $C_P^{FeO_{1.5}}$ and C_P^{FeO} from Lange and Navrotsky (1992) and C_p of O_2 gas from JANAF (Chase, 1998) at a reference temperature of 1673 K gives $\Delta C_p = 32.5$ J/K.

In empirical form, Eq. (14) reduces to

$$\frac{\Delta G_{T,P_0}}{RT} = a + \frac{b}{T} + c\ln T \tag{15}$$

where $c = -\Delta C_p$ Representations similar to Eqs. (14) and (15) include Kress and Carmichael (1991), Jayasuriya et al. (2004) (their Eq. (10) plus "ΔG(1)"), and Deng et al. (2020). The value of ΔC_P also imparts a constant and reciprocal temperature influence, which can either be folded into the a and b terms in an empirical fit (Eqs. (14) and (15)), or included separately (Kress and Carmichael, 1991):

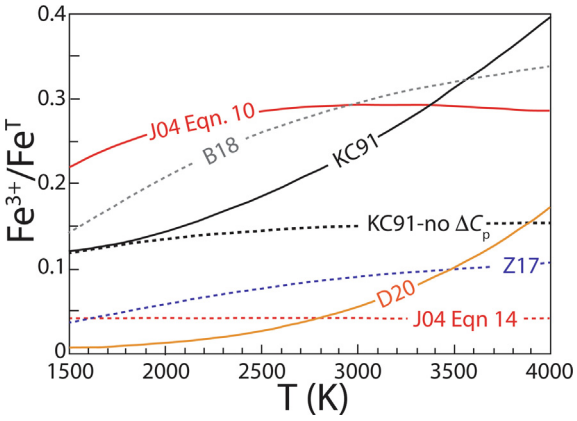

Fig. 4. Calculated temperature variations of Fe^{3+}/Fe^T from different thermodynamic models (Kress and Carmichael, 1991; Jayasuriya et al., 2004; Zhang et al., 2017; Borisov et al., 2018; Deng et al., 2020) for liquid with a composition of the bulk silicate Earth (McDonough and Sun, 1995) at f_{O2} fixed at IW−2. Except for Eq. (14) of Jayasuriya et al. (2004) (see text), models that incorporate non-zero values of ΔCp (solid lines) predict increases in Fe^{3+}/Fe^T at high temperature, whereas those that assume $\Delta Cp = 0$ (dashed lines) approach constant values. This is illustrated by calculating two curves for the Kress and Carmichael (1991) model; one that includes the ΔC_p term and one that excludes it. Note that for the curves in these plots, only the temperature dependences and not the absolute values of Fe^{3+}/Fe^T are relevant. This is because the Fe^{3+}/Fe^T predicted by each model is influenced by the adopted activity coefficients, which in most cases are not accurate for ultramafic liquids (Fig. 3).

$$\frac{\Delta G_{T,P_0}}{RT} = a + \frac{b}{T} - \Delta C_p\left(1 + \frac{T_0}{T} + ln\left(\frac{T}{T_0}\right)\right) \tag{16}$$

where T_0 is a reference temperature (1673 K). The inclusion of the ΔC_P term has relatively little influence on calculated Fe^{3+}/Fe^T at temperatures of most experimental measurements, but becomes significant in extrapolation to high temperature. This is demonstrated in Fig. 4 in which the model of Kress and Carmichael (1991) is calculated for a peridotite liquid at IW−2 as originally formulated (ΔC_P = 27.9 J/K) and with ΔC_P omitted. The two are little-different below 2000 K, but diverge above, and at 4000 K, the calculation that excludes the ΔC_P term predicts Fe^{3+}/Fe^T of 0.015, whereas including the term predicts Fe^{3+}/Fe^T of 0.04, more than twice as great.

Both the functions of Kress and Carmichael (1991) and Deng et al. (2020), which adopt values of ΔC_P guided by calorimetry of FeO and $FeO_{1.5}$ liquid components, predict significant increases in Fe^{3+}/Fe^T when extrapolated to high temperature (Fig. 4). The third model that incorporates a dependence on ΔC_P, Jayasuriya et al. (2004) (Eq. (10) plus "ΔG(1)"), does not show a similar trend because the value of ΔC_P employed, −3.124 J/K, is of opposite sign and an order of magnitude smaller than that derived from experimental determinations (e.g., Lange and Navrotsky, 1992). We conclude that based on present knowledge of the heat capacities of FeO and $FeO_{1.5}$ in silicate liquids, the effects of high temperature in deep magma oceans should enhance Fe^{3+}/Fe^T significantly.

A second source of temperature dependence to Fe^{3+}/Fe^{T} is possible variations in activity coefficients. Some previous models (Sack et al., 1980; Kress and Carmichael, 1991; Zhang et al., 2017; Borisov et al., 2018) have adopted athermal compositional terms (which assume that non-ideality between iron species and other melt components has no temperature dependence). Because these are derived from experimental data that span a relatively small temperature interval, temperature effects on non-ideality may not be significant, and, if present, are manifested in regressed terms nominally associated with $\Delta G_{T,P_0}$. Other models (Jayasuriya et al., 2004; Eq. (14); Deng et al., 2020) adopt temperature-dependent non-ideality terms derived from regular solution theory. These follow the well-established expectation that thermodynamic non-ideality diminishes with temperature (Pitzer and Brewer, 1961) and are consistent with other general considerations of the temperature effect on non-ideality in silicate liquids, such as closing of miscibility gaps, whether they arise from regular-solution-like interactions or speciation (Hess, 1995; Navrotsky, 1995). Although experimental data on the effects of non-ideality on Fe^{3+}/Fe^{T} at very high temperature are lacking, models that incorporate a diminishing effect with temperature are likely more appropriate in temperature extrapolation.

3.3. Effect of pressure

Depending on differences in the partial molar volumes of ferrous and ferric oxide components in silicate melts, pressure can either enhance or diminish the stability of Fe^{3+}. The change in volume of condensed components in reaction (9) is given by

$$\Delta\bar{V}_x = \bar{V}_{FeO_{1.5}} - \bar{V}_{FeO} \quad (17)$$

and is comparatively large at low pressures (Lange and Carmichael, 1987), such that at fixed temperature and oxygen fugacity relative to Fe-O-Si buffers (IW, quartz-fayalite-magnetite), Fe^{3+}/Fe^{T} diminishes with pressure (Kress and Carmichael, 1991; O'Neill et al., 2006; Zhang et al., 2017). However, owing to the greater compressibility of $FeO_{1.5}$ relative to FeO, this trend reverses at higher pressures, leading to increases in Fe^{3+}/Fe^{T} (Hirschmann, 2012; Armstrong et al., 2019; Deng et al., 2020).

Contrary to the assertion of Armstrong et al. (2019), the value of $\Delta\bar{V}_x$ need not become negative to produce a positive Fe^{3+}/Fe^{T} trend with pressure at an f_{O2} fixed relative to IW or other buffer. Rather, $\Delta\bar{V}_x$ should simply be smaller than that compared to the $\Delta\bar{V}$ for the buffer reaction. Along isopleths of constant f_{O2} relative to the IW buffer, Fe^{3+} in silicate melt will be stabilized by increased pressure if

$$\Delta\bar{V}_x < \frac{1}{2}\left(\bar{V}_{FeO} - \bar{V}_{Fe}\right) \quad (18)$$

The factor of ½ arises because $\Delta\bar{V}_x$ is associated with liberation or fixation of ¼ mole of O_2 (Eq. (9)) whereas the IW reaction (Eq. (1)) involves ½ mole. Of importance to the discussion in the following paragraph, the sign of $\Delta\bar{V}_x$ should remain positive at all reasonable conditions, as the volume of $FeO_{1.5}$, with 1.5 oxygens per formula unit, should exceed that of FeO, with one.

Quantitative evaluation of the effect of pressure on Fe^{3+}/Fe^{T} in silicate melts depends on an appropriate thermal equation of state to evaluate the integral

$$\int_{P_0}^{P} \bar{V}\, dP \quad (19)$$

Among available EOS, only those of Armstrong et al. (2019) and Deng et al. (2020) extend to pressures sufficiently great to capture the key decrease of Fe^{3+}/Fe^{T} with pressure that was predicted by Hirschmann (2012). Armstrong et al. (2019) calibrated a Tait EOS from experiments up to 23 GPa, whereas Deng et al. (2020) derived a 4th order Birch-Murnaghan (B-M) EOS from volumes of idealized silicate components, determined by first principles methods. However, owing to very high predicted compressibility of $FeO_{1.5}$, extrapolation of the Tait EOS of Armstrong et al. (2019) above 10 GPa produces physically implausible negative values for $\Delta\bar{V}_x$(Fig. S1A) and above the pressures of their experimental calibration (≤23 GPa), this leads to large and unreasonable predicted values of Fe^{3+}/Fe^{T} (Fig. S1B). Therefore, whereas both may feasibly apply to modest pressures applicable to Mars, Deng et al. (2020) gives at present the only viable EOS plausibly applicable to core-forming conditions relevant to Earth (≥28 GPa, Table 1,Fig. 2).

3.4. A revised model

Here we formulate a revised model that predicts Fe^{3+}/Fe^{T} in ultramafic liquids at conditions relevant to deep magma oceans. Although our interests are limited to ultramafic compositions, the revised model accounts for the effects of compositional variation as this is needed to calibrate the effects of temperature on Fe^{3+}/Fe^{T}. In order to derive an accurate temperature dependence, it is preferable to span the full range of experimental temperatures available (1468–2197 K), and this requires modeling composition effects also, as the high temperature liquids are ultramafic and those at low temperature are mafic.

As a starting point, we take the model of Borisov et al. (2018), owing to its relative success in predicting Fe^{3+}/Fe^{T} in peridotitic liquids (Fig. 3),

$$\log\left(\frac{X_{FeO_{1.5}}}{X_{FeO}}\right) = 0.207\log f_{O_2} - 10,852 + 4633.3/T + \left[\begin{array}{c} -0.445X_{SiO_2} - 0.9X_{TiO_2} + 1.532X_{MgO} + 0.314X_{CaO} + 2.03X_{Na_2O} + \\ 3.355X_{K_2O} - 4.851X_{P_2O_5} - 3.081X_{SiO_2}X_{Al_2O_3} - 4.370X_{SiO_2}X_{MgO} \end{array}\right] \quad (20)$$

We modify Eq. (20) in four ways: (1) we incorporate a term for ΔC_p, using the form adopted by Kress and Carmichael (1991) and the difference in partial molar heat capacities of $FeO_{1.5}$ and FeO (33.25 J/K) from Lange and Navrotsky (1992), (2) we employ single-cation oxide mole fractions, rather than integer oxygen units, (3) we assume

that the non-ideal contributions are proportional to reciprocal temperature and (4) we adopt a pressure dependence based either the equations of state of Armstrong et al. (2019) or Deng et al. (2020).

$$\log\left(\frac{X_{FeO_{1.5}}}{X_{FeO}}\right) = a\log f_{O_2} + b + \frac{c}{T} - \frac{\Delta C_p}{R\ln(10)}\left[1 - \frac{T_0}{T} - \ln\left(\frac{T}{T_0}\right)\right] - \frac{\int_{P_0}^{P}\Delta V dP}{RT\ln(10)} + \frac{1}{T}\begin{bmatrix} Y_1X_{SiO_2} + Y_2X_{TiO_2} + Y_3X_{MgO} + Y_4X_{CaO} + Y_5X_{NaO_{0.5}} \\ +Y_6X_{KO_{0.5}} + Y_7X_{PO_{2.5}} + Y_8X_{SiO_2}X_{AlO_{1.5}} + Y_9X_{SiO_2}X_{MgO} \end{bmatrix} \quad (21)$$

Choosing a relation for which the dependence on $\log f_{O2}$ is an adjustable parameter (a) (Eq. (12)), rather than the canonical value of (1/4) (Eq. (11)), has a small effect on calculations extrapolated to reduced conditions applicable to magma oceans, as elaborated in the Discussion (Section 6.1). Next, we calibrate the adjustable terms in Eq. (21) (a, b, c, y_i) at 100 kPa from a least squares regression, using the database of wet chemical analyses compiled by Borisov et al. (2018), Mössbauer determinations for andesite and MORB melts over a wide range of f_{O2}s (Cottrell et al., 2009; Zhang et al., 2016; Zhang et al., 2018), and the XANES analyses of peridotite glasses of Sossi et al. (2020). These total 478 experiments spanning 1468–2197 K. The reduced χ^2_v for the fit is 4.38, but this relatively high value is attributable to the Mössbauer-analyzed samples. For those analyzed by wet chemistry (n = 435), the reduced χ^2_v is 2.71. As shown in Fig. 5, the quality of the fits for glasses analyzed by Mössbauer and wet chemistry are not obviously different, and so the distinction is likely owing to smaller estimated uncertainties for Mössbauer Fe^{3+}/Fe^{T}, which could be underestimates.

The high pressure experiments of O'Neill et al. (2006), Zhang et al. (2017) and Armstrong et al. (2019) can be used to examine the relative performances of the Armstrong et al. (2019) and Deng et al. (2020) EOS at modest pressures. As shown in Fig. S2, neither model reproduces the experiments with high accuracy – both tend to underpredict Fe^{3+}/Fe^{T} at low pressure (<5 GPa). Above 15 GPa, the models diverge, with the Armstrong and Deng EOS predicting values of Fe^{3+}/Fe^{T} that are higher than and lower than experimental values, respectively. In the case of the Armstrong EOS, this is attributable to the exaggerated compressibility of $FeO_{1.5}$ (Fig. S1).

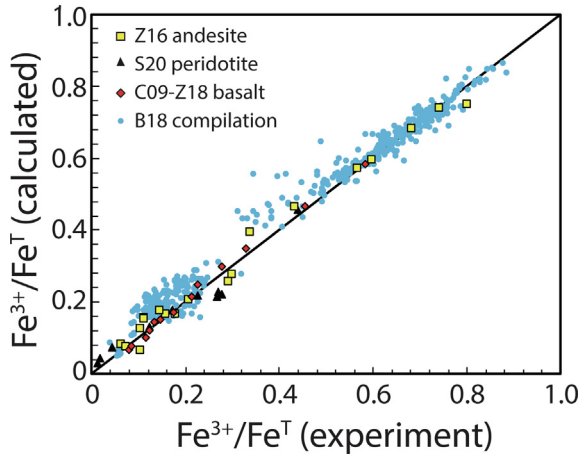

Fig. 5. Comparison of Fe^{3+}/Fe^{T} from experimental glasses to calculated with Eq. (21) and parameter values in Table 2. Experimental data include wet chemical analyses compiled by Borisov et al. (2018) (B19, n = 435), andesites from Zhang et al. (2016) (Z16, n = 19), basalts from Cottrell et al. (2009), with revised Fe^{3+}/Fe^{T} from Zhang et al. (2018) (C09-Z18, n = 14), and peridotite glasses from Sossi et al. (2020) (S20, n = 10, glasses from time series were excluded). Overall fit has a reduced χ^2_v of 4.38.

4. IMPORTANCE OF CR

4.1. Cr redox in magma oceans and solidified upper mantle

As noted in the Introduction, Cr in a magma ocean equilibrated with alloy is present as Cr^{2+} (Corgne et al., 2008; Mann et al., 2009; Siebert et al., 2011; Steenstra et al., 2020), but in the upper mantles of Earth in Mars, Cr is chiefly Cr^{3+}. On crystallization of the upper mantle, some Fe^{3+} is converted to Cr^{3+} according to reaction (2) and so the amount of Fe^{3+} in crystallized upper mantles should be less than that present in the magma ocean from which they descend. We focus on Cr as it is the only lithophile element in silicate melts apart from Fe known with some certainty to a adopt a different valence state than in solidified mantle and that is present in abundances sufficient to have appreciable effect on Fe via intervalence reactions. It is conceivable that Ti could contribute a similar, though smaller effect, as considered further in Section 6.4 of the Discussion.

To calculate the fraction of magma ocean Fe^{3+} that is converted to Fe^{2+} during solidification of the upper mantles on Earth and Mars from reaction (2), we consider the proportion of Cr^{3+} that is present at relevant f_{O2} and temperature for spinel peridotite, which we take as typical of the many source regions for terrestrial and martian basalts, (Falloon et al., 2008; Filiberto, 2017) and therefore a principal source of constraints on mantle f_{O2}. At the f_{O2} values relevant for the terrestrial and martian upper mantles, we consider that the pyroxene and spinel incorporate only Cr^{3+} (Papike et al., 2005), though under highly reduced conditions sufficient to stabilize Cr metal (~IW−4), both phases also incorporate Cr^{2+} (Li et al., 1995). We calculate the Cr^{2+}/Cr^{3+} ratio in olivine as a function of temperature and f_{O2}, as detailed below. Therefore, mass balance gives the concentration of Cr in bulk spinel peridotite, C_T^{Cr}, as a function of the mass modes of the constituent minerals, m_i,

$$C_T^{Cr} = C_T^{Cr^{2+}} + C_T^{Cr^{3+}} \quad (22)$$

$$C_T^{Cr^{2+}} = m_{ol}C_{ol}^{Cr^{2+}} \quad (23)$$

$$C_T^{Cr^{3+}} = m_{ol}C_{ol}^{Cr^{3+}} + m_{opx}C_{opx}^{Cr^{3+}} + m_{cpx}C_{cpx}^{Cr^{3+}} + m_{spl}C_{spl}^{Cr^{3+}} \quad (24)$$

Concentrations of Cr in pyroxenes and spinel are calculated from applicable mineral/olivine partition coefficients, $D_{Cr}^{i/ol}$:

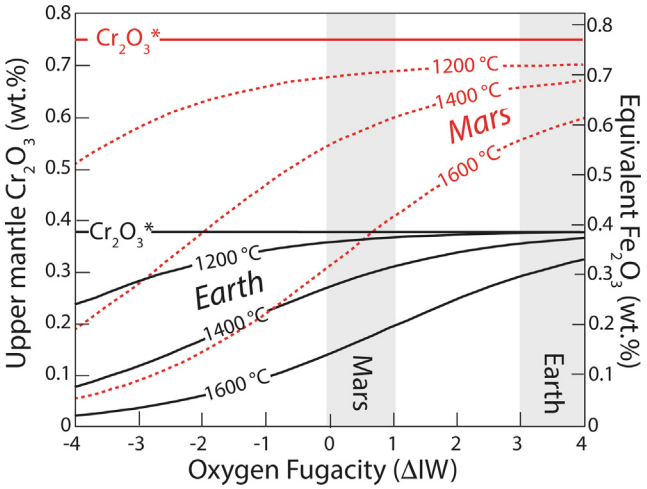

Fig. 6. Cr present as Cr_2O_3 in spinel peridotite upper mantle of Earth and Mars as a function of f_{O2} and temperature, calculated from Eq. (27). The calculation assumes 0.38 wt.% total Cr_2O_3* for Earth and 0.75 wt.% for Mars (Table 1). Shaded regions show f_{O2} of primitive basalt source regions in terrestrial upper mantle of Earth and Mars, with the latter relevant only to the most reducing basalts. Along the right-hand Y axis is the scale for Fe_2O_3 that is reduced to FeO in proportion of a given Cr_2O_3 concentration, according to reaction (2). As the atomic weights of Fe and Cr are little different, this is hardly distinguishable from the Cr_2O_3 scale.

$$C_{opx}^{Cr^{3+}} = D_{Cr}^{opx/ol} C_{ol}^{Cr^{3+}};\ C_{cpx}^{Cr^{3+}} = D_{Cr}^{cpx/ol} C_{ol}^{Cr^{3+}};\ C_{spl}^{Cr^{3+}} = D_{Cr}^{spl/ol} C_{ol}^{Cr^{3+}} \quad (25a, b, c)$$

and Cr^{2+} in olivine is calculated from the Cr^{2+}/Cr^{3+} ratio

$$C_{ol}^{Cr^{2+}} = \left(\frac{C_{ol}^{Cr^{2+}}}{C_{ol}^{Cr^{3+}}}\right) C_{ol}^{Cr^{3+}} \quad (26)$$

Combining and rearranging Eqs. (22)–(26) gives

$$C_T^{Cr^{3+}} = \frac{C_T^{cr}\left(m_{ol} + m_{opx} D_{Cr}^{opx/ol} + m_{cpx} D_{cr}^{cpx/ol} + m_{spl} D_{cr}^{spl/ol}\right)}{\left[m_{ol}\left(\frac{C_{ol}^{Cr^{2+}}}{C_{ol}^{Cr^{3+}}} + 1\right) + m_{opx} D_{Cr}^{opx/ol} + m_{cpx} D_{cr}^{cpx/ol} + m_{spl} D_{cr}^{spl/ol}\right]} \quad (27)$$

We take the mineral modes of terrestrial and martian mantles from Bertka and Holloway (1994) and inter-mineral partitioning is given by the temperature-dependent expressions (Hervig and Smith, 1982):

$$\ln D_{Cr^{3+}}^{opx/ol} = \frac{5540}{T} - 1.86 \text{ (Hervig and Smith, 1982)} \quad (28)$$

$$\ln D_{Cr^{3+}}^{cpx/ol} = \frac{8787}{T} - 2.87 \text{ (Hervig and Smith, 1982)} \quad (29)$$

$$\ln D_{Cr^{3+}}^{spl/ol} = \frac{10,358}{T} - 1.45, \quad (30)$$

where the latter is an empirical recasting of the relation in Witt-Eickschen and O'Neill (2005), which was given in terms of spinel Cr#. We calculate the Cr^{2+}/Cr^{3+} ratio in olivine as a function of f_{O2}, modified from the isothermal formulation of Jollands et al. (2018)

$$\frac{C_{ol}^{Cr^{2+}}}{C_{ol}^{Cr^{3+}}} = 10^{-(0.25\left(\frac{\Delta}{W} + IW_{P0}\right) + \log K)} \quad (31)$$

where K is the equilibrium constant for the Cr^{2+}/Cr^{3+} exchange reaction in olivine (Eq. (25) in Jollands et al., 2018), IW_{P0} is the log f_{O2} of IW at the temperature of interest and 100 kPa (Hirschmann, 2021) and ΔIW is the difference between the log f_{O2} of interest and the IW buffer. For log K, Jollands et al. (2018) used a value of 1.84 at 1400 °C, but here we adopt a temperature dependence based on the calibration of Li et al. (1995) for the Cr^{2+} concentration in olivine in equilibrium with chromian spinel.

$$\log K = \frac{13,319}{T} - 6.117 \quad (32)$$

Eqs. (31) and (32) assume that Cr^{2+}/Cr^{T} does not vary with pressure at fixed relative f_{O2} (i.e., along fugacity isopleths parallel to the IW buffer). According to Li et al. (1995), pressure should cause small decreases in the concentration of Cr^{2+} in olivine at fixed relative f_{O2}.

The mineral/olivine partition coefficient expressions in Eqs. (28)–(30) are presumed to apply to partitioning of Cr^{3+} only, as they are derived empirically from xenoliths which equilibrated at low temperatures where Cr^{2+} in olivine can be neglected (Li et al., 1995). If these empirical Cr partition coefficients are affected by some Cr^{2+} in olivine, they underestimate $D_{Cr}^{i/ol}$ for Cr^{3+}, and therefore they underestimate the amount of Cr^{3+} in the calculated bulk rock. These calculations also make the simplified assumption of constant mineral modes for Earth and Martian mantles. They therefore do not account for several factors that likely affect these modes, though the effect of these variable modes on peridotite Cr^{3+}/Cr^{T} are small compared to the effects of f_{O2} and temperature. These factors include: (1) Different proposed compositions of the martian mantle (Table 1) should correspond to slightly different modes. (2) mineral modes in the spinel peridotite facies are affected by temperature and pressure (3). In detail, the spinel mode depends on whole rock Cr_2O_3 and Fe_2O_3 and therefore on f_{O2}.

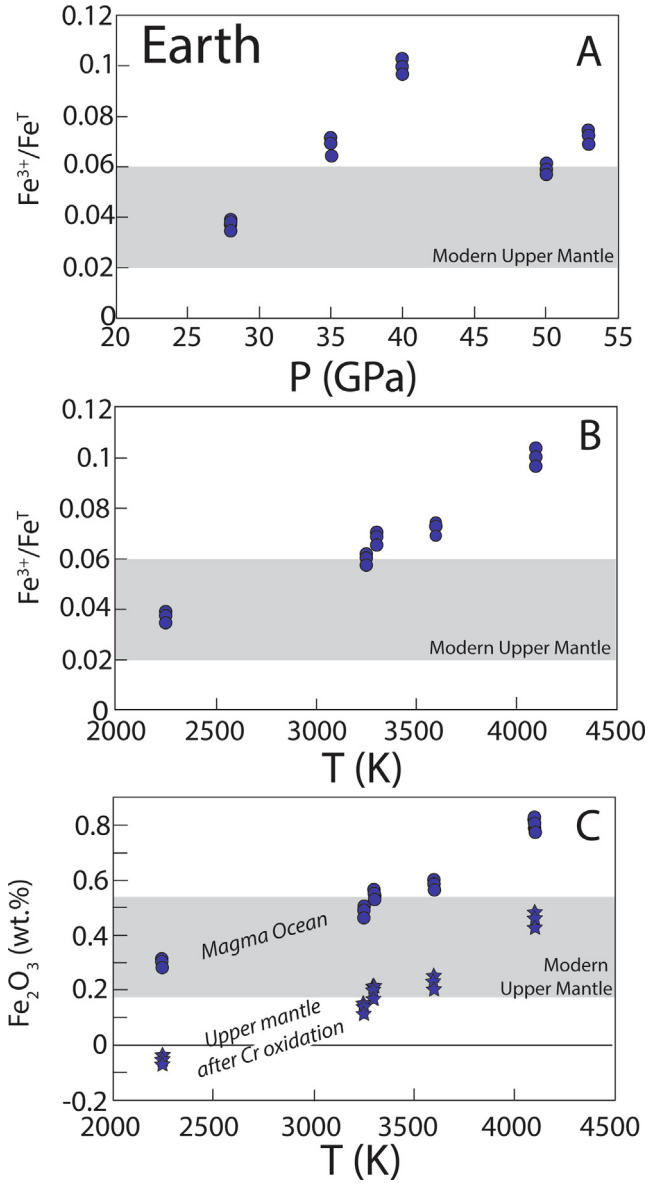

Fig. 7. Calculated Fe^{3+}/Fe^{T} of a terrestrial magma ocean, calculated for different proposed magma ocean-core equilibration conditions (Table 1; Fig. 2) versus pressure (A) and temperature (B). Shaded region shows range of Fe^{3+}/Fe^{T} (0.02–0.06) proposed for Earth's modern upper mantle (Canil et al., 1994; Canil and O'Neill, 1996; Cottrell and Kelley, 2011; Gaetani, 2016; O'Neill et al., 1993; Sossi et al., 2020; Woodland et al., 2006). Panel C shows the same calculations translated to total Fe_2O_3. It also shows the Fe_2O_3 that would remain following destruction of 0.35% Fe_2O_3 by oxidation of CrO in the magma ocean to Cr_2O_3 during mantle crystallization. Negative calculated values of Fe^{3+}/Fe^{T} signify oversaturation with alloy (see main text).

As shown in Fig. 6, the Cr^{3+} content of the upper mantle increases with oxygen fugacity and decreases with temperature. With increasing temperature, the greater stability of Cr^{2+} in olivine (Eq. (32)) combines with a weaker tendency of Cr to partition into pyroxene and spinel (Eqs. (28)–(30)) to suppress Cr^{3+} stability. For oxygen fugacities relevant to Earth's upper mantle (>IW+3), nearly all available Cr is Cr^{3+} (>0.3 wt.% Cr_2O_3). For those applicable to the primitive martian upper mantle (IW – IW+1), at least 0.3 wt% Cr is present as Cr_2O_3 at high temperature (1600 °C), and 0.5–0.6 wt.% at 1400 °C. As Cr_2O_3 and Fe_2O_3 have nearly the same molecular weights, comparable masses of Fe_2O_3 must be consumed in reaction (2) to produce these quantities of Cr_2O_3 (Fig. 6).

5. RESULTS

5.1. Application to Fe^{3+}/Fe^{T} in magma oceans

For terrestrial magma ocean conditions (Table 1, Fig. 2) the Fe^{3+}/Fe^{T} predicted using the Deng et al. (2020) EOS ranges from 0.034 to 0.103 (Fig. 7A,B), which for mantle

with 8 wt.% FeO* (Table 1) translates to 0.28–0.83 wt.% Fe_2O_3 (Fig. 7C). Both pressure and temperature enhance Fe^{3+}/Fe^T (Figs. 4, S1), but comparison of Fig. 7A and B shows that temperature has the greatest control, with the largest ratios predicted for the highest temperature magma ocean conditions. Thus, the Fe^{3+}/Fe^T predicted from core segregation of the terrestrial magma ocean is similar to or greater than that present in the upper mantle today (0.02–0.06; Fig. 7). However, as discussed below, a significant fraction of the Fe^{3+} produced in the magma ocean may be destroyed during crystallization by intervalence transfer with Cr.

For martian magma ocean conditions, the Fe^{3+}/Fe^T predicted is 0.029–0.038 for the Deng et al. (2020) EOS and 0.026–0.034 for the Armstrong et al. EOS (Fig. 8A). The corresponding concentrations of Fe_2O_3 depend on the assumed total FeO* of the martian mantle, and span from 0.37 wt.% for a magma ocean with 13.5 wt.% FeO* up to 0.68 wt.% with 18.1 wt.% FeO* (Fig. 8B). The positive correlation of Fe^{3+}/Fe^T with FeO* is owing to the influence of the latter on oxygen fugacity (Fig. 2). The concentrations of Fe_2O_3 prevailing in the modern martian upper mantle are not well-known, but these predicted Fe^{3+}/Fe^T ratios are comparable to the low to middle range of estimates for Earth's upper mantle (Fig. 7A), and should be more than sufficient to account for the modest oxidation of the solid martian mantle (IW or greater). However, the influence of Cr during crystallization will affect these relationships significantly, as considered below.

5.2. From magma ocean to solid upper mantle, with Cr oxidation

Taking conservative estimates of Fe_2O_3 consumed by Cr oxidation during upper mantle crystallization to be 0.35 wt.% for Earth and 0.55 wt.% for Mars (Fig. 6), the amount of Fe_2O_3 remaining in solidified upper mantle is considerably less than that set at magma ocean conditions. For Earth, the remaining Fe_2O_3 can be similar to the low to intermediate estimates of modern upper mantle concentrations if magma ocean-metal equilibration occurred at high temperature (>3300 K) (Fig. 7C). For Mars, remaining Fe_2O_3 is negative for lower estimates of bulk mantle FeO* (Fig. 8B). Negative concentrations are unphysical and

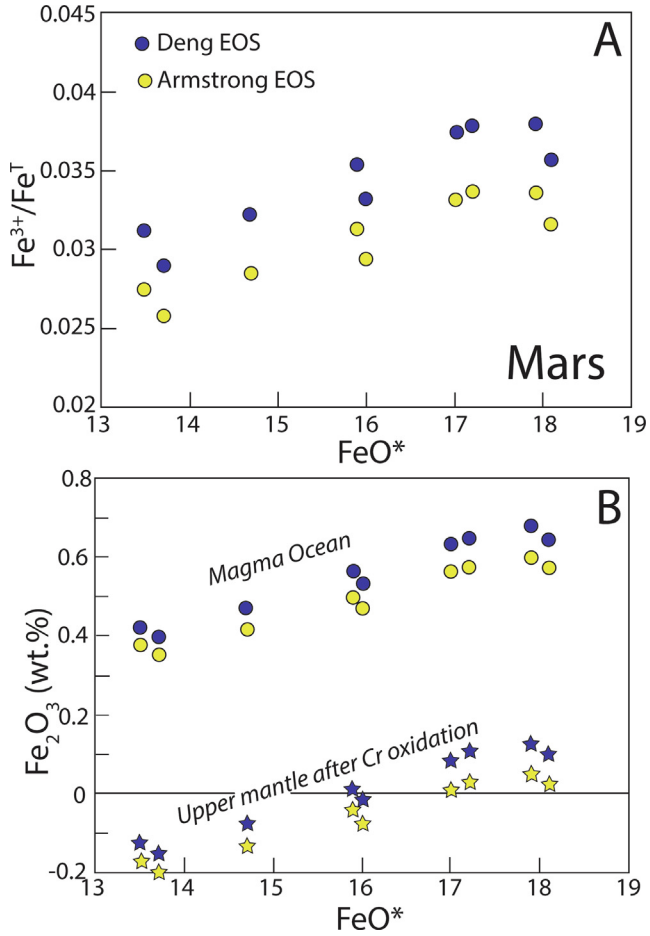

Fig. 8. Calculated (A) Fe^{3+}/Fe^T and (B) Fe_2O_3 of a martian magma ocean, calculated for conditions of proposed core-mantle equilibration and for different proposed FeO* contents of the martian mantle (Table 1; Fig. 2). Panel B also shows the Fe_2O_3 that would remain following destruction of 0.55% Fe_2O_3 by oxidation of CrO in the magma ocean to Cr_2O_3 during mantle crystallization.

imply over-saturation of Fe-rich alloy, which in turn would impose oxygen fugacities at least below IW−1. Small positive concentrations of Fe_2O_3, required for conditions as oxidized as IW (i.e., peridotite unsaturated in alloy), are feasible only for martian bulk mantle compositions with ≥17 wt.% FeO*.

6. DISCUSSION

6.1. Choice of Fe^{3+}/Fe^T fit equation and extrapolation to reduced conditions

As accurate measurement of low Fe^{3+}/Fe^T ratios in silicate glasses is challenging, thermodynamic models of Fe^{3+}/Fe^T are by necessity largely based on extrapolation from experiments conducted at comparatively oxidized conditions. Therefore, the extrapolated values depend not only on the quality of the fit to experimental data, but also on the functional form of the adopted equation; e.g. Eq. (11) versus Eq. (12). This difference can be illustrated by comparison of the predicted 100 kPa values for peridotite liquid from the model in this work (Eq. (21); Table 2), which has the form of Eq. (12), and the simple parameterization of Sossi et al. (2020), which has a log f_{O2} dependence of 0.25, as in Eq. (11).

From their 100 kPa experiments, Sossi et al. (2020) regressed the relationship

$$\log(Fe^{3+}/Fe^{2+}) = 0.252\Delta IW - 1.53 \quad (33)$$

However, Sossi et al. (2020) calculated IW from O'Neill and Eggins (2002), which takes reference states of crystalline iron and molten FeO and this combination of solid and liquid reference phases convolves the buffer with a fusion reaction. When extrapolated to high temperature, this has the effect of overstabilizing FeO and yielding a low f_{O2} value for the Fe-FeO boundary. Therefore, whereas Sossi et al. (2020) took log(IW) to be −6.47 at 2173 K, the accurate value is −5.97 (O'Neill and Pownceby, 1993; Hirschmann, 2021). We therefore correct Eq. (33) as

$$\log(Fe^{3+}/Fe^{2+}) = 0.252\Delta IW - 1.4. \quad (34)$$

As shown in Fig. 9, at reducing conditions Eq. (21) predicts larger values of Fe^{3+}/Fe^T than the corrected Sossi et al. (2020) relation (Eq. (34)). At conditions most relevant to the calculations in this paper (IW−2 to IW−1), the Fe^{3+}/Fe^T difference is ~0.015. The Sossi et al. (2020) parameterization fits better the peridotite experiments from low f_{O2} in part because Eq. (21) is calibrated from a large number of experiments (Fig. 5), whereas Eq. (34) is calibrated solely from the peridotite experiments in that study. We note however, that the apparent low values of Fe^{3+}/Fe^T for the reduced experimental glasses in Sossi et al. (2020) derive from a XANES calibration based on Berry et al. (2018). The Berry et al. (2018) calibration is derived from an *a priori* assumption that reduced basaltic glasses have zero Fe_2O_3, and is debated in the literature (Borisov et al., 2018; O'Neill et al., 2018; Zhang et al., 2018; Cottrell et al., 2021). The merits of this debate are mostly beyond the scope of the present contribution. However, as made clear by the work on which this study is based (Armstrong et al., 2019; Deng et al., 2020), the Fe_2O_3 content of reduced silicate liquids is not zero at high pressure, and there is no theoretical reason why it must be absent at lower pressure. Regardless, adoption by Sossi et al. (2020) of the Berry et al. (2018) XANES calibration minimizes apparent Fe^{3+}/Fe^T in reduced low pressure glasses. If the thermodynamic model adopted here were more similar to that of Sossi et al. (2020), the calculated magma ocean values of Fe^{3+}/Fe^T would be approximately 0.015 lower than described in Section 5.1, and this would not change significantly the inferences and conclusions here about magma ocean ferric iron. On the other hand, for the same Fe^{3+}/Fe^T, Eq. (34) predicts ΔIW more oxidized than Eq. (21). For values of Fe^{3+}/Fe^T of 0.02, 0.04, and 0.06, the respective differences are 1.3, 0.9, and 0.7 log units. This may have appreciable effect on the f_{O2} of an atmosphere overlying a magma ocean, as discussed below in Section 6.3.

Table 2
Fit parameters for calculating $\log(FeO_{1.5}/FeO)$ in silicate melts from Eq. (21).

Parameter	Value	Units
a	0.1917	
b	−1.961	
c	4158.1	K
ΔCp	33.25	J/K
T_0	1673.15	K
y_1	−520.46	K
y_2	−185.37	K
y_3	494.39	K
y_4	1838.34	K
y_5	2888.48	K
y_6	3473.68	K
y_7	−4473.6	K
y_8	−1245.09	K
y_9	−1156.86	K

Fit at 100 kPa. $\chi^2_v = 4.38$ ($n = 478$).

6.2. Extrapolation and the need for further experiments

We emphasize that the thermodynamic calculations in this work are in important instances extrapolations in temperature, pressure and melt composition compared to existing experimental constraints. The recent experimental results for peridotitic liquids at 100 kPa (Sossi et al., 2020) show well that most previous models, based on mafic liquids, do not predict accurately the Fe^{3+}/Fe^T of melt compositions relevant to magma oceans (Fig. 3). Further, the effects of both elevated pressure and temperature are both important for accurate assessment of Fe^{3+}/Fe^T in magma oceans (Figs. 4, S2). Though temperatures and pressures relevant to core segregation on Mars are spanned by present experimental data, those applicable to Earth must be extrapolated beyond existing observational temperature and pressure constraints. This highlights the need for experiments at more extreme conditions and for melt compositions relevant to magma oceans.

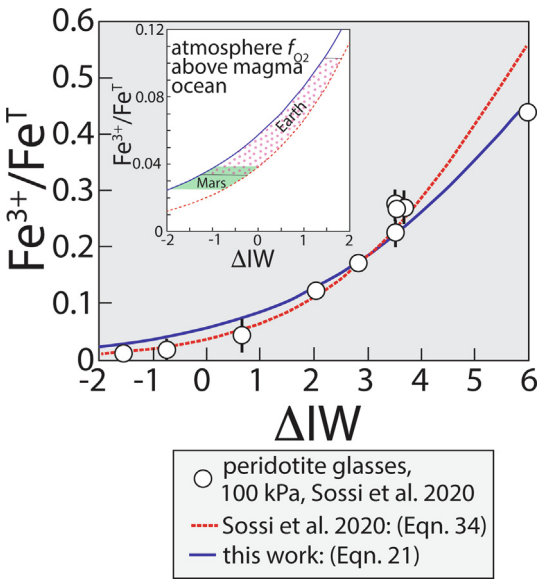

Fig. 9. Fe^{3+}/Fe^{T} of peridotite liquid at 100 kPa and 2173 K calculated from the model in this work (Eq. (21), Table 2) and the corrected model of Sossi et al. (2020) (Eq. (34)). Also shown are peridotite liquid experiments from Sossi et al. at 2112–2197 K, with 2σ uncertainty bars where these exceed symbol size. Note that the ΔIW scale here, based on crystalline iron and wüstite (Hirschmann, 2021) is different from that employed by Sossi et al. (2020) (see main text), that the latter at 2173 K is 0.5 log units more reduced, and so corresponding values of ΔIW are 0.5 units higher. **Inset** shows the span of values of ΔIW for the atmospheres above magma oceans on Earth (stippled region) and Mars (green region), corresponding to the plausible ranges of Fe^{3+}/Fe^{T} for each magma ocean (Figs. 6, 7) and the differing models (Eqs. (21) and (34)), calculated at 2173 K.

6.3. An oxidized magma ocean atmosphere?

One of the consequences of stabilization of Fe_2O_3 in a magma ocean is that it may impose oxidizing conditions on the overlying atmosphere (Hirschmann, 2012). Sossi et al. (2020) argued that the atmosphere above Earth's magma ocean would be modestly oxidizing (corrected value ΔIW = 0, see Section 6.1), based on the assumption that the Fe^{3+}/Fe^{T} of the magma ocean was 0.037 ± 0.005, the same as their estimate of Earth's present-day upper mantle. Destruction of magma ocean Fe_2O_3 by Cr oxidation is just one reason why the modern mantle and magma ocean Fe^{3+}/Fe^{T} may not be the same. Forward modeling of Fe^{3+} stabilized in the magma ocean environment (Figs. 6, 7) allows further exploration of this question.

The relationship between magma ocean Fe_2O_3 and f_{O2} at its surface differs depending on the model used for calculation (Fig. 9). For a terrestrial magma ocean with Fe^{3+}/Fe^{T} ratios of 0.034–0.103 (Fig. 7), the corresponding f_{O2} ranges from IW−1.2 to IW+1.4 using Eq. (21) from this study, or −0.2 to 1.8 for the corrected relationship of Sossi et al. (2020) (Eq. (34)) (Fig. 9 Inset). For a martian magma ocean (Fe^{3+}/Fe^{T} = 0.026–0.038, Fig. 8), the corresponding values are IW−1.4 to −0.7 from Eq. (21) and −0.4 to 0.2 from Eq. (34) (Fig. 9 Inset). These results affirm that an oxidized atmosphere, composed chiefly of H_2O and CO_2, is feasible above Earth's magma ocean and that an intermediate atmosphere composed of CO, CO_2, H_2O, and H_2, may be possible above a martian magma ocean. However, the range of plausible oxidation states highlights that the combined uncertainties in magma ocean Fe_2O_3 contents and in the relationship between magma ocean Fe^{3+}/Fe^{T} and low pressure f_{O2} remain too great to establish with certainty the redox state and composition of atmospheres above magma oceans on Earth and Mars.

6.4. Ferric iron in crystallized mantle following Fe-Cr redox exchange

The thermodynamic calculations above show that at plausible conditions of magma ocean-molten alloy equilibration for Earth and Mars, significant Fe_2O_3 should be produced and that these Fe_2O_3 concentrations can be equal to or greater than that present in the upper mantles of these planets today. The range of core-forming conditions explored for Earth (Fig. 7C) illustrates that temperature is a key parameter enhancing magma ocean Fe_2O_3, whilst the range of mantle compositions considered for Mars (Fig. 8B) highlights that more Fe_2O_3 is produced for more FeO*-rich mantles, in which metal-silicate equilibration produces more oxidized conditions. However, the fractions of Fe_2O_3 stabilized in molten mantle are not necessarily preserved upon crystallization.

A key consideration is that in a magma ocean equilibrated with metal, chromium is present as CrO, whereas at plausible redox conditions in the upper mantles of Earth and Mars, much of it is Cr_2O_3. Thus, a significant portion of the Fe_2O_3 present in parcels of magma ocean that crystallize to form material destined for planetary upper mantles is destroyed by Cr oxidation. This effect does not depend on direct crystallization of the upper mantle from a magma ocean. For example, magma ocean crystallization at greater depth, where Cr_2O_3 stability may not be the same as calculated in Fig. 6, may retain greater amounts of Fe_2O_3 together with CrO in silicate minerals (See discussion in Supplementary Information). However, on later advection of that material to the upper mantle, conversion of CrO to Cr_2O_3 will reduce the same fraction of Fe_2O_3 as indicated in Fig. 6.

The stabilization of Fe_2O_3 in a hot deep magma ocean, followed by destruction of much or even all of that ferric iron by oxidation of Cr in crystallized upper mantle peridotite are two key processes that affect the oxidation states of the upper mantles of Earth and Mars. Whether these result in the comparatively oxidized character of basalt source regions on these planets depends on factors such as the temperature and pressure of metal-silicate equilibration and the abundance of total mantle iron. If the thermodynamic models adopted here are accurate, then this combination of processes could result in appropriate quantities of solidified mantle Fe_2O_3 if mean conditions of core formation on Earth and Mars are at sufficient temperature and pressure, and for the case of Mars, if the mantle FeO* content is great enough. As recent geophysical data from the InSight mission point to martian mantle FeO* contents

at the lower end of the range depicted in Fig. 8 (Khan et al., 2022), other processes such as hydrogen degassing seem required.

6.5. The possible role of Ti

Like Cr, Ti also could feasibly participate in charge transfer reactions during magma ocean solidification and thereby affect the redox evolution from core segregation to crystallized mantle. In solidified terrestrial and martian upper mantles, Ti is present only as Ti^{4+}, though a small fraction of Ti^{3+} is present in the more reduced lunar mantle (Papike et al., 2005), In reduced silicate liquids some studies have suggested that a portion of Ti could be present as Ti^{3+} (Schreiber et al., 1978; Borisov, 2012). Conversion of Ti^{3+} present during core segregation to Ti^{4+} following mantle solidification would have an effect similar to that of Cr, destroying a portion of the Fe^{3+} stabilized during magma ocean solidification,

$$\underset{\text{magma}}{Fe_2O_3} + \underset{\text{magma}}{Ti_2O_3} \Longleftrightarrow 2\ \underset{\text{peridotite}}{TiO_2} + 2\ \underset{\text{peridotite}}{FeO} \quad (35)$$

Concentrations of Ti in the terrestrial (0.2 wt.% TiO_2; McDonough and Sun, 1995) and martian mantles (0.1–0.3 wt.% TiO_2; Yoshizaki and McDonough, 2020) are less than those for Cr (Table 1) and if only a portion of the Ti in a magma ocean is Ti^{3+}, then the overall effect of Ti would be to enhance modestly the Cr-induced destruction of Fe^{3+} during magma ocean crystallization. However, whether there was appreciable Ti^{3+} in silicate melt equilibrated with alloy in the magma oceans of these planets is not clearly established.

Early experiments at 100 kPa on simple-system silicate melt compositions in which Ti^{3+} concentrations were evaluated by wet chemistry, infrared spectroscopy, or thermodynamic inference suggested the presence of modest fractions of Ti^{3+} below IW (see review by Borisov, 2012). More recent Ti-XANES studies of (Fe-free) lunar analog glasses have failed to find appreciable Ti^{3+} even at conditions as reduced as IW−7 (Leitzke et al., 2018; Tarragó et al., 2022). Experimental studies of silicate/alloy partitioning of Ti at conditions relevant to core formation have inferred that Ti is essentially all Ti^{4+} (Kilburn and Wood, 1998; Corgne et al., 2008; Steenstra et al., 2020), though these interpretations are complicated by the influence of Si on Ti partitioning at highly reduced conditions (Kilburn and Wood, 1997; Steenstra et al., 2020). More experimental and analytical work is likely required to quantify if Ti^{3+} influences magma ocean redox balance at prevailing temperatures, pressures, melt compositions and oxygen fugacities, but at present evidence is insufficient to conclude that Ti has a significant role.

6.6. Other factors influencing magma ocean and early mantle redox

We focus here on FeO-Fe_2O_3 equilibria in magma oceans and CrO-Cr_2O_3 intervalence transfer during upper mantle crystallization, two key factors influencing the redox conditions in terrestrial planets as they evolve from the magma ocean stage to the first solidified mantle, but other processes are also likely to contribute, including subsolidus iron disproportionation, late accretion, and hydrogen degassing, which we discuss below. The first two of these would not affect Fe redox in the magma ocean, but would modify Fe^{3+}/Fe^{T} of the crystallized mantle. Hydrogen degassing could oxidize the magma ocean itself. Beyond these, yet additional processes, including magma ocean differentiation (Schaefer and Elkins-Tanton, 2018), carbon oxidation (Canil and O'Neill, 1996; Stagno et al., 2013), and long-term secular evolution owing to mantle-surface exchange (Aulbach et al., 2019; Nicklas et al., 2019) or to mantle cooling (Gaetani, 2016) could be factors, but are not considered further here.

Prior to the hypothesis that Fe_2O_3 could be stabilized in a deep magma ocean (Hirschmann, 2012), it was established that Earth's early mantle could have become oxidized by Fe_2O_3 produced by iron disproportionation during crystallization of high pressure minerals (Mao, 1974; Frost et al., 2004; Wade and Wood, 2005; Frost and McCammon, 2008). Frost et al. (2004) argued that stabilization of Fe^{3+} in bridgmanite formed during magma ocean crystallization drove precipitation of an iron-rich phase that was subsequently removed to the core as a S-rich liquid. This crystallization-driven disproportionation could also be expected from a Fe_2O_3-containing magma ocean if the Fe^{3+}/Fe^{T} of precipitating bridgmanite was greater than that of the coexisting silicate liquid.

If bridgmanite Fe^{3+}/Fe^{T} is greater than the magma ocean from which it crystallizes, the remaining liquid Fe^{3+}/Fe^{T} diminishes. Depending on whether this shift is greater than the decrease in Fe^{3+}/Fe^{T} at alloy saturation with diminishing temperature (Figs. 4, 6B), alloy would also precipitate and thereby produce additional Fe_2O_3. Indirect experimental evidence suggests that this could be the case; i.e., Fe^{3+}/Fe^{T} in bridgmanite crystallized at IW−2 near 25 GPa and 2000 K is approximately 0.2 (Frost et al., 2004; Terasaki et al., 2007; Boujibar et al., 2016), significantly greater than that expected for peridotitic liquid at similar conditions (Fig. 7). This mechanism would not be applicable to Mars if bridgmanite is not stable in the deeper parts of the martian mantle (Stahler et al., 2021).

Another factor possibly influencing redox conditions in early planetary mantles is late accretion post-dating magma ocean crystallization. The effects of late accretion depend in part on the character of accreting material. Accretion of reduced bodies similar to non-carbonaceous (NC) chondrites would add metal, tending to reduce the mantle (Pahlevan et al., 2019), whereas the iron in carbonaceous (CC) chondrites is approximately equal parts FeO and Fe_2O_3 (Sutton et al., 2017) and could oxidize it. Nicklas et al. (2021) argued that the comparatively oxidized character of the martian mantle is owing to late accretion of oxidized chondritic material. Late accretion for Earth and Mars amounted to approximately 1% of mantle masses (Walker, 2009; Tait and Day, 2018). Assuming accreting bodies were 25 wt.% FeO* similar to typical chondrites (Jarosewich, 2006), and neglecting the reducing effect of associated organic carbon, then late accretion of purely enstatite (NC) chondrites would diminish the Earth's bulk

mantle Fe^{3+}/Fe^{T} of Earth's bulk mantle (8 wt.% FeO*, Table 1) by 0.06. For martian mantle with 13–18 wt.% FeO, the decrease would be 0.03–0.04. Late accretion of CC devoid of organic carbon could have a more modest effect in the opposite direction, increasing Fe^{3+}/Fe^{T} by 0.014 for Earth and 0.006–0.008 for Mars.

On the basis of Ru and Mo isotopes, late accreted material for Mars and for much of Earth is thought to have been largely NC, though for Earth some fraction of CC is permissible (Hopp et al., 2020; Kleine et al., 2020). Considering only late-accreted iron, an admixture of consisting of 80% carbonaceous and 20% enstatite chondrite-like material would have an approximately neutral effect, and contributions from late-accreted organic carbon make it likely that even 100% CC late-accretion would diminish the Fe^{3+}/Fe^{T} ratio that persisted following crystallization of the terrestrial and martian magma oceans. Though quantification awaits better-resolved constraints on the relative mass fractions of CC and NC accreting late to Earth and Mars, the processes responsible for the comparatively oxidized condition of crystallized upper mantles of Earth and Mars likely had to overcome the reducing effects of late accretion.

An additional process leading to oxidation of magma oceans and early planetary mantles is hydrogen escape (Hunten, 1973; Dreibus and Wanke, 1987; Hamano et al., 2013; Sharp et al., 2013; Sharp, 2017; Pahlevan et al., 2019). Dissociation of dissolved H_2O in a magma ocean to hydrogen gas (e.g., Hirschmann et al., 2012) drives the reaction

$$\underset{\text{melt}}{H_2O} + 2\underset{\text{melt}}{FeO} \iff \underset{\text{gas}}{H_2} + \underset{\text{melt}}{Fe_2O_3} \tag{36}$$

Assuming that Earth's water originated from a reservoir with D/H ratio similar to that of chondrites, Pahlevan et al. (2019) calculated that the mass of hydrogen degassed from the magma ocean was limited to <2 MPa atmospheric pressure. This modest loss would enhance the Fe^{3+}/Fe^{T} in Earth's mantle by up to ~0.025. The magnitude of hydrogen escape and consequent magma ocean oxidation on Mars is not as easily constrained, in part because of large variations in D/H between martian surface and interior reservoirs (Usui et al., 2015; Peslier et al., 2019; Barnes et al., 2020).

7. CONCLUDING REMARKS

Recalculated conditions of core formation on Earth relative to the crystalline iron-wustite buffer range from ΔIW−1.4 to ΔIW−2.5, with more reduced conditions corresponding to greater temperature. For Mars, ΔIW of core formation ranges from −1.6 to −1.2, depending on the assumed FeO* of the magma ocean.

Melt composition, temperature, and pressure are all important factors determining the Fe^{3+}/Fe^{T} ratio in deep magma oceans equilibrated with core-destined alloy. We have calibrated a new thermodynamic model that is based on experiments with both mafic and ultramafic melt composition and that facilitates extrapolation to high temperature, taking into account differences in liquid FeO and $FeO_{1.5}$ heat capacities. Combined with available equations of state, application of this model for representative deep magma ocean conditions for Earth and Mars predicts Fe^{3+}/Fe^{T} ratios of 0.034–0.10 and 0.026–0.038 respectively. Higher ratios are possible if hydrodynamic escape of hydrogen occurred from overlying atmospheres during the magma ocean stage. Atmospheres above magma oceans on Earth and Mars could have been comparatively oxidized if temperatures of the terrestrial magma ocean were at the high end of likely conditions and if the martian mantle is more FeO*-rich. However, such conditions would have limited the partial pressure of H_2, thereby diminishing the efficacy of further magma ocean oxidation by hydrodynamic escape.

Oxygen fugacities and Fe^{3+}/Fe^{T} ratios prevailing in magma oceans are unlikely to translate directly to those in crystallized mantle, as additional redox processes occur during and immediately after magma ocean crystallization. One such process, not previously considered, is oxidation of Cr^{2+} to Cr^{3+} during magma ocean crystallization, which has the potential to consume much or even all of the Fe_2O_3 produced in a deep magma ocean. For Earth, this could leave sufficient Fe^{3+} in the upper mantle to account for present-day redox if core formation occurred at the higher end of feasible temperatures and pressures. For Mars, the Cr-Fe redox exchange has the potential to destroy virtually all the Fe^{3+} produced by magma ocean processes unless the martian mantle FeO* is at the high end of proposed values.

Late accretion is likely to reduce the early mantles of Earth and Mars, as isotopic evidence favors metal-bearing NC material predominating and as the reduction potential of metal-bearing chondrite-like compositions, per unit mass, is significantly greater than the oxidation potential of impactors similar to carbonaceous chondrites. On Earth, disproportionation of FeO to Fe_2O_3 + Fe during bridgmanite crystallization may have had a significant oxidizing effect. Thus, the redox conditions of young planetary mantles are a product of a combination of processes. Yet, the role of high pressure is significant, first in stabilizing Fe_2O_3 in the magma ocean and second in promoting disproportionation during bridgmanite crystallization, and favors more oxidized conditions in larger terrestrial planets.

Declaration of Competing Interest

The authors declare that they have no known competing financial interests or personal relationships that could have appeared to influence the work reported in this paper.

ACKNOWLEDGEMENTS

I gratefully acknowledge support from NSF (EAR2016215) and NASA (80NSSC21K1826 and 80NSSC21K1826). I thank Hongluo Zhang, Tony Withers, Jie Deng, and Sanath Aithala for motivating discussions. Alexander Borisov and an anonymous referee provided constructive reviews that improved the final version of this paper. Jie Deng graciously shared Python code which calculates the Deng et al. (2020) equation of state and which I used as a template for some of the MATLAB scripts used here.

APPENDIX A. SUPPLEMENTARY MATERIAL

Supplementary material to this article can be found online at https://doi.org/10.1016/j.gca.2022.04.005.

REFERENCES

Armstrong K., Frost D. J., McCammon C. A., Rubie D. C. and Ballaran T. B. (2019) Deep magma ocean formation set the oxidation state of Earth's mantle. *Science* **365**, 903–906.

Aulbach S., Woodland A. B., Stern R. A., Vasilyev P., Heaman L. M. and Viljoen K. S. (2019) Evidence for a dominantly reducing Archaean ambient mantle from two redox proxies, and low oxygen fugacity of deeply subducted oceanic crust. *Sci. Reports* **9**, 20190.

Badro J., Côté A. S. and Brodholt J. P. (2014) A seismologically consistent compositional model of Earth's core. *Proc. Nat. Acad. Sci.* **111**, 7542–7545.

Barnes J. J., McCubbin F. M., Santos A. R., Day J. M. D., Boyce J. W., Schwenzer S. P., Ott U., Franchi I. A., Messenger S., Anand M. and Agee C. B. (2020) Multiple early-formed water reservoirs in the interior of Mars. *Nat. Geosci.* **13**, 260.

Berry A. J., Stewart G. A., O'Neill H. S. C., Mallmann G. and Mosselmans J. F. W. (2018) A re-assessment of the oxidation state of iron in MORB glasses. *Earth Planet. Sci. Lett.* **483**, 114–123.

Bertka C. M. and Holloway J. R. (1994) Anhydrous partial melting of an iron-rich mantle. 1. Subsolidus phase assemblages and partial melting phase-relations at 10 to 30 kbar. *Contrib. Mineral. Petrol.* **115**, 313–322.

Borisov A., Behrens H. and Holtz F. (2018) Ferric/ferrous ratio in silicate melts: A new model for 1atm data with special emphasis on the effects of melt composition. *Contrib. Mineral. Petrol.* **173**, 98.

Borisov A. A. (2012) The Ti^{4+}/Ti^{3+} ratio of magmatic melts: Application to the problem of the reduction of lunar basalts. *Petrology* **20**, 391–398.

Boujibar A., Bolfan-Casanova N., Andrault D., Bouhifd M. A. and Trcera N. (2016) Incorporation of Fe^{2+} and Fe^{3+} in bridgmanite during magma ocean crystallization. *Am. Mineral.* **101**, 1560–1570.

Campbell A. J., Danielson L., Righter K., Seagle C. T., Wang Y. B. and Prakapenka V. B. (2009) High pressure effects on the iron-iron oxide and nickel-nickel oxide oxygen fugacity buffers. *Earth Planet. Sci. Lett.* **286**, 556–564.

Canil D. (2002) Vanadium in peridotites, mantle redox and tectonic environments: Archean to present. *Earth Planet. Sci. Lett.* **195**, 75–90.

Canil D. and O'Neill H. S. C. (1996) Distribution of ferric iron in some upper-mantle assemblages. *J. Petrol.* **37**, 609–635.

Canil D., O'Neill H. S., Pearson D. G., Rudnick R. L., McDonough W. F. and Carswell D. A. (1994) Ferric iron in peridotites and mantle oxidation-states. *Earth Planet. Sci. Lett.* **123**, 205–220.

Chase M. W. (1998) NIST-JANAF Themochemical Tables, 4th ed. American Institute of Physics.

Chi H., Dasgupta R., Duncan M. S. and Shimizu N. (2014) Partitioning of carbon between Fe-rich alloy melt and silicate melt in a magma ocean – Implications for the abundance and origin of volatiles in Earth, Mars, and the Moon. *Geochim. Cosmochim. Acta* **139**, 447–471.

Corgne A., Keshav S., Wood B. J., McDonough W. F. and Fei Y. (2008) Metal-silicate partitioning and constraints on core composition and oxygen fugacity during Earth accretion. *Geochim. Cosmochim. Acta* **72**, 574–589.

Cottrell E., Birner S. K., Brounce M., Davis F. A., Waters L. E. and Kelley K. A. (2021) Oxygen fugacity across tectonic settings. In *Magma Redox Geochemistry* (eds. R. Moretti and D. R. Neuville). Wiley, pp. 33–61.

Cottrell E. and Kelley K. A. (2011) The oxidation state of Fe in MORB glasses and the oxygen fugacity of the upper mantle. *Earth Planet. Sci. Lett.* **305**, 270–282.

Cottrell E., Kelley K. A., Lanzirotti A. and Fischer R. A. (2009) High-precision determination of iron oxidation state in silicate glasses using XANES. *Chem. Geol.* **268**, 167–179.

Davis F. A. and Cottrell E. (2021) Partitioning of Fe_2O_3 in peridotite partial melting experiments over a range of oxygen fugacities elucidates ferric iron systematics in mid-ocean ridge basalts and ferric iron content of the upper mantle. *Contrib. Mineral. Petrol.* **176**, 67.

Deguen R., Landeau M. and Olson P. (2014) Turbulent metal-silicate mixing, fragmentation, and equilibration in magma oceans. *Earth Planet. Sci. Lett.* **391**, 274–287.

Delano J. W. (2001) Redox history of the Earth's interior since similar to 3900 Ma: Implications for prebiotic molecules. *Orig. Life Evol. Biosph.* **31**, 311–341.

Deng J., Du Z. X., Karki B. B., Ghosh D. B. and Lee K. K. M. (2007) A magma ocean origin to divergent redox evolutions of rocky planetary bodies and early atmospheres. *Nature Comm.* **11**, 2007.

Doyle C. D. (1988) Prediction of the activity of FeO in multicomponent magma from known values in SiO_2-$KAlO_2$-$CaAl_2Si_2O_8$-FeO liquids. *Geochim. Cosmochim. Acta* **52**, 1827–1834.

Dreibus G. and Wanke H. (1987) Volatiles on Earth and Mars – a comparison. *Icarus* **71**, 225–240.

Falloon T. J., Green D. H., Danyushevsky L. V. and McNeill A. W. (2008) The composition of near-solidus partial melts of fertile peridotite at 1 and 1.5 GPa: Implications for the petrogenesis of MORB. *J. Petrol.* **49**, 591–613.

Filiberto J. (2017) Geochemistry of Martian basalts with constraints on magma genesis. *Chem. Geol.* **466**, 1–14.

Fischer R. A., Campbell A. J., Shofner G. A., Lord O. T., Dera P. and Prakapenka V. B. (2011) Equation of state and phase diagram of FeO. *Earth Planet. Sci. Lett.* **304**, 496–502.

Frost D. J. (2003) Fe^{2+}-Mg partitioning between garnet, magnesiowustite, and $(Mg, Fe)_2SiO_4$ phases of the transition zone. *Am. Mineral.* **88**, 387–397.

Frost D. J., Liebske C., Langenhorst F., McCammon C. A., Tronnes R. G. and Rubie D. C. (2004) Experimental evidence for the existence of iron-rich metal in the Earth's lower mantle. *Nature* **428**, 409–412.

Frost D. J., Mann U., Asahara Y. and Rubie D. C. (2008) The redox state of the mantle during and just after core formation. *Phil. Trans. Roy. Soc. A* **366**, 4315–4337.

Frost D. J. and McCammon C. A. (2008) The redox state of Earth's mantle. *Ann. Rev. Earth Planet Sci.* **36**, 389–420.

Gaetani G. A. (2016) The behavior of Fe^{3+}/Sigma Fe during partial melting of spinel lherzolite. *Geochim. Cosmochim. Acta* **185**, 64–77.

Gessmann C. K. and Rubie D. C. (2000) The origin of the depletions of V, Cr and Mn in the mantles of the Earth and Moon. *Earth Planet. Sci. Lett.* **184**, 95–107.

Gessmann C. K., Wood B. J., Rubie D. C. and Kilburn M. R. (2001) Solubility of silicon in liquid metal at high pressure: Implications for the composition of the Earth's core. *Earth Planet. Sci. Lett.* **184**, 367–376.

Hamano K., Abe Y. and Genda H. (2013) Emergence of two types of terrestrial planet on solidification of magma ocean. *Nature* **497**, 607–611.

Herd C. D. K. (2008) Basalts as probes of planetary interior redox state. *Rev. Mineral. Geochem.* **68**, 527–553.

Hervig R. L. and Smith J. V. (1982) Temperature-dependent distribution of Cr between olivine and pyroxenes in lherzolite xenoliths. *Contrib. Mineral. Petrol.* **81**, 184–189.

Hess P. C. (1995) Thermodynamic mixing properties and the structure of silicate melts. *Rev. Mineral. Geochem.* **32**, 145–189.

Hidayat T., Shishin D., Jak E. and Decterov S. A. (2015) Thermodynamic reevaluation of the Fe-O system. *Calphad-Computer Coupling Phase Diagrams Thermochem.* **48**, 131–144.

Hirschmann M. M. (2012) Magma ocean influence on early atmosphere mass and composition. *Earth Planet. Sci. Lett.* **341**, 48–57.

Hirschmann M. M. (2021) Iron-wüstite revisited: A revised calibration accounting for variable stoichiometry and the effects of pressure. *Geochim. Cosmochim. Acta* **313**, 74–84.

Hirschmann M. M., Withers A. C., Ardia P. and Foley N. T. (2012) Solubility of molecular hydrogen in silicate melts and consequences for volatile evolution of terrestrial planets. *Earth Planet. Sci. Lett.* **345**, 38–48.

Holzheid A. and Grove T. L. (2005) The effect of metal composition on Fe-Ni partition behavior between olivine and FeNi-metal, FeNi-carbide, FeNi-sulfide at elevated pressure. *Chem. Geol.* **221**, 207–224.

Hopp T., Budde G. and Kleine T. (2020) Heterogeneous accretion of Earth inferred from Mo-Ru isotope systematics. *Earth Planet. Sci. Lett.* **534**, 116065.

Hunten D. M. (1973) Escape of light gases from planetary atmospheres. *J. Atmos. Sci.* **30**, 1481–1494.

Jarosewich E. (2006) Chemical analyses of meteorites at the Smithsonian Institution: An update. *Meteorit. Planet. Sci.* **41**, 1381–1382.

Jayasuriya K. D., O'Neill H. S., Berry A. J. and Campbell S. J. (2004) A Mössbauer study of the oxidation state of Fe in silicate melts. *Am. Mineral.* **89**, 1597–1609.

Jollands M. C., O'Neill H. S. C., Van Orman J., Berry A. J., Hermann J., Newville M. and Lanzirotti A. (2018) Substitution and diffusion of Cr^{2+} and Cr^{3+} in synthetic forsterite and natural olivine at 1200–1500 degrees C and 1 bar. *Geochim. Cosmochim. Acta* **220**, 407–428.

Khan A., Liebske C., Rozel A., Rivoldini A., Nimmo F., Connolly J. A. D., Plesa A. C. and Giardini D. (2018) A geophysical perspective on the bulk composition of Mars. *J. Geophys. Res.-Planets* **123**, 575–611.

Khan A., Sossi P., Liebske C., Rivoldini A. and Giardini D. (2022) Geophysical and cosmochemical evidence for a volatile-rich Mars. *Earth Planet. Sci. Lett.* **578**, 117330.

Khan A. and Connolly J. A. D. (2008) Constraining the composition and thermal state of Mars from inversion of geophysical data. *Journal of Geophysical Research-Planets* **113**, E07003.

Kilburn M. R. and Wood B. J. (1997) Metal-silicate partitioning and the incompatibility of S and Si during core formation. *Earth Planet. Sci. Lett.* **152**, 139–148.

Kilburn M. R. and Wood B. J. (1998) The Effect of oxygen fugacity and silicate melt composition on the partitioning of titanium, vanadium, chromium, and manganese between liquid metal and silicate melt, The Origin of the Earth and the Moon. *LPI Contrib.* **957**, 18.

Kleine T., Budde G., Burkhardt C., Kruijer T. S., Worsham E. A., Morbidelli A. and Nimmo F. (2020) The non-carbonaceous-carbonaceous meteorite dichotomy. *Space Sci. Rev.* **216**, 55.

Komabayashi T. (2014) Thermodynamics of melting relations in the system Fe-FeO at high pressure: Implications for oxygen in the Earth's core. *J. Geophys. Res.-Solid Earth* **119**, 4164–4177.

Kowalski M. and Spencer P. J. (1995) Thermodynamic reevaluation of the Cr-O, Fe-O and Ni-O systems – remodeling of the liquid, b*cc* and f*cc* phases. *Calphad-Computer Coupling Phase Diagrams Thermochem.* **19**, 229–243.

Kress V. C. and Carmichael I. S. E. (1991) The compressibility of silicate liquids containing Fe_2O_3 and the effect of composition, temperature, oxygen fugacity and pressure on their redox states. *Contrib. Mineral. Petrol.* **108**, 82–92.

Lange R. A. and Carmichael I. S. E. (1987) Densities of Na_2O-K_2O-CaO-MgO-FeO-Fe_2O_3-Al_2O_3-TiO_2-SiO_2 liquids – new measurements and derived partial molar properties. *Geochim. Cosmochim. Acta* **51**, 2931–2946.

Lange R. A. and Navrotsky A. (1992) Heat-capacities of Fe_2O_3-bearing silicate liquids. *Contrib. Mineral. Petrol.* **110**, 311–320.

Leitzke F. P., Fonseca R. O. C., Gottlicher J., Steininger R., Jahn S., Prescher C. and Lagos M. (2018) Ti K-edge XANES study on the coordination number and oxidation state of Titanium in pyroxene, olivine, armalcolite, ilmenite, and silicate glass during mare basalt petrogenesis. *Contrib. Mineral. Petrol.* **173**, 103.

Li J. and Agee C. B. (1996) Geochemistry of mantle-core differentiation at high pressure. *Nature* **381**, 686–689.

Li J. and Agee C. B. (2001) The effect of pressure, temperature, oxygen fugacity and composition on partitioning of nickel and cobalt between liquid Fe-Ni-S alloy and liquid silicate: Implications for the Earth's core formation. *Geochim. Cosmochim. Acta* **65**, 1821–1832.

Li J. P., O'Neill H. S. C. and Seifert F. (1995) Subsolidus phase-relations in the system MgO-SiO_2-Cr-O in equilibrium with metallic Cr, and their significance for the petrochemistry of chromium. *J. Petrol.* **36**, 107–132.

Liebske C. and Khan A. (2019) On the principal building blocks of Mars and Earth. *Icarus* **322**, 121–134.

Litasov K. D. and Shatskiy A. F. (2016) Composition of the Earth's core: A review. *Geologiya i geofizika* **57**, 31–62.

Lock S. J. and Stewart S. T. (2017) The structure of terrestrial bodies: Impact heating, corotation limits, and synestias. *J. Geophys. Res.-Planets* **122**, 950–982.

Lodders K. and Fegley B. (1997) An oxygen isotope model for the composition of Mars. *Icarus* **126**, 373–394.

Longhi J. (2006) Petrogenesis of picritic mare magmas: Constraints on the extent of early lunar differentiation. *Geochim. Cosmochim. Acta* **70**, 5919–5934.

Ma Z. T. (2001) Thermodynamic description for concentrated metallic solutions using interaction parameters. *Metall. Mat. Trans. B* **32**, 87–103.

Mann U., Frost D. J. and Rubie D. C. (2009) Evidence for high-pressure core-mantle differentiation from the metal-silicate partitioning of lithophile and weakly-siderophile elements. *Geochim. Cosmochim. Acta* **73**, 7360–7386.

Mao H. K. (1974) A discussion of the iron oxides at high pressures with implications for the chemical and thermal evolution of the earth. *Carnegie Inst. Wash. Yearbook* **73**, 510–518.

McDonough W. (2003). *Compositional model for the Earth's core. Treatise on geochemistry 2*. Elsevier, pp. 547–568.

McDonough W. F. and Sun S. S. (1995) The composition of the Earth. *Chem. Geol.* **120**, 223–253.

Morgan J. W. and Anders E. (1979) Chemical composition of Mars. *Geochim. Cosmochim. Acta* **43**, 1601–1610.

Navrotsky A. (1995) Energetics of silicate melts. *Rev. Mineral. Geochem.* **32**, 121–143.

Nicklas R. W., Day J. M. D., Vaci Z., Udry A., Liu Y. and Tait K. T. (2021) Uniform oxygen fugacity of shergottite mantle sources and an oxidized martian lithosphere. *Earth Planet. Sci. Lett.* **564**, 116876.

Nicklas R. W., Puchtel I. S., Ash R. D., Piccoli P. M., Hanski E., Nisbet E. G., Waterton P., Pearson D. G. and Anbar A. D. (2019) Secular mantle oxidation across the Archean-Proterozoic boundary: Evidence from V partitioning in komatiites and picrites. *Geochim. Cosmochim. Acta* **250**, 49–75.

Norris C. A. and Wood B. J. (2017) Earth's volatile contents established by melting and vaporization. *Nature* **549**, 507–511.

O'Neill H. S., Berry A. J. and Mallmann G. (2018) The oxidation state of iron in Mid-Ocean Ridge Basaltic (MORB) glasses: Implications for their petrogenesis and oxygen fugacities. *Earth Planet. Sci. Lett.* **504**, 152–162.

O'Neill H. S. C., Berry A. J., McCammon C. C., Jayasuriya K. D., Campbell S. J. and Foran G. (2006) An experimental determination of the effect of pressure on the Fe^{3+}/Sigma Fe ratio of an anhydrous silicate melt to 3.0 GPa. *Am. Mineral.* **91**, 404–412.

O'Neill H. S. C. and Eggins S. M. (2002) The effect of melt composition on trace element partitioning: An experimental investigation of the activity coefficients of FeO, NiO, CoO, MoO_2 and MoO_3 in silicate melts. *Chem. Geol.* **186**, 151–181, Pii s0009-2541(01)00414-4.

O'Neill H. S. C., McCammon C. A., Canil D., Rubie D. C., Ross C. R. and Seifert F. (1993) Mössbauer-spectroscopy of mantle transition zone phases and determination of minimum Fe^{3+} content. *Am. Mineral.* **78**, 456–460.

O'Neill H. S. and Pownceby M. I. (1993) Thermodynamic data from redox reactions at high-temperatures. 1. An experimental and theoretical assessment of the electrochemical method using stabilized zirconia electrolytes, with revised values for the Fe-FeO, CO-CoO, Ni-NiO AND Cu-Cu_2O oxygen buffers, and new data for the W-WO_2 buffer. *Contrib. Mineral. Petrol.* **114**, 296–314.

Pahlevan K., Schaefer L. and Hirschmann M. M. (2019) Hydrogen isotopic evidence for early oxidation of silicate Earth. *Earth Planet. Sci. Lett.* **526**, 115770.

Papike J. J., Karner J. M. and Shearer C. K. (2005) Comparative planetary mineralogy: Valence state partitioning of Cr, Fe, Ti, and V among crystallographic sites in olivine, pyroxene, and spinel from planetary basalts. *Am. Mineral.* **90**, 277–290.

Peslier A. H., Hervig R., Yang S., Humayun M., Barnes J. J., Irving A. J. and Brandon A. D. (2019) Determination of the water content and D/H ratio of the martian mantle by unraveling degassing and crystallization effects in nakhlites. *Geochim. Cosmochim. Acta* **266**, 382–415.

Pitzer K. and Brewer L. (1961) Thermodynamics, 2nd ed. McGraw Hill.

Rai N. and van Westrenen W. (2013) Core-mantle differentiation in Mars. *J. Geophys. Res.-Planets* **118**, 1195–1203.

Righter K., Danielson L. R., Pando K. M., Williams J., Humayun M., Hervig R. L. and Sharp T. G. (2015) Highly siderophile element (HSE) abundances in the mantle of Mars are due to core formation at high pressure and temperature. *Meteorit. Planet. Sci.* **50**, 604–631.

Righter K. and Drake M. J. (1996) Core formation in Earth's Moon, Mars, and Vesta. *Icarus* **124**, 513–529.

Righter K., Rowland, II, R., Danielson L. R., Humayun M., Yang S., Mayer N. and Pando K. (2020) Mantle-melt partitioning of the highly siderophile elements: New results and application to Mars. *Meteorit. Planet. Sci.* **55**, 2741–2757.

Rubie D. C., Frost D. J., Mann U., Asahara Y., Nimmo F., Tsuno K., Kegler P., Holzheid A. and Palme H. (2011) Heterogeneous accretion, composition and core-mantle differentiation of the Earth. *Earth Planet. Sci. Lett.* **301**, 31–42.

Rubie D. C., Gessmann C. K. and Frost D. J. (2004) Partitioning of oxygen during core formation on the Earth and Mars. *Nature* **429**, 58–61.

Sack R. O., Carmichael I. S. E., Rivers M. and Ghiorso M. S. (1980) Ferric-ferrous equilibria in natural silicate liquids at 1bar. *Contrib. Mineral. Petrol.* **75**, 369–376.

Santos A. R., Agee C. B., McCubbin F. M., Shearer C. K., Burger P. V., Tartese R. and Anand M. (2015) Petrology of igneous clasts in Northwest Africa 7034: Implications for the petrologic diversity of the martian crust. *Geochim. Cosmochim. Acta* **157**, 56–85.

Schaefer L. and Elkins-Tanton L. T. (2018) Magma oceans as a critical stage in the tectonic development of rocky planets. *Phil. Trans. Roy. Soc. A* **376**, 20180109.

Schmidt M. E., Schrader C. M. and McCoy T. J. (2013) The primary f_{O2} of basalts examined by the Spirit rover in Gusev Crater, Mars: Evidence for multiple redox states in the martian interior. *Earth Planet. Sci. Lett.* **384**, 198–208.

Schreiber H. D., Thanyasiri T., Lach J. J. and Legere R. A. (1978) Redox equilibria of Ti, Cr, and Eu in silicate melts – reduction potentials and mutual interactions. *Phys. Chem. Glasses* **19**, 126–139.

Sharp Z. D. (2017) Nebular ingassing as a source of volatiles to the terrestrial planets. *Chem. Geol.* **448**, 137–150.

Sharp Z. D., McCubbin F. M. and Shearer C. K. (2013) A hydrogen-based oxidation mechanism relevant to planetary formation. *Earth Planet. Sci. Lett.* **380**, 88–97.

Siebert J., Badro J., Antonangeli D. and Ryerson F. J. (2012) Metal-silicate partitioning of Ni and Co in a deep magma ocean. *Earth Planet. Sci. Lett.* **321**, 189–197.

Siebert J., Badro J., Antonangeli D. and Ryerson F. J. (2013) Terrestrial accretion under oxidizing conditions. *Science* **339**, 1194–1197.

Siebert J., Corgne A. and Ryerson F. J. (2011) Systematics of metal-silicate partitioning for many siderophile elements applied to Earth's core formation. *Geochim. Cosmochim. Acta* **75**, 1451–1489.

Snyder G. A., Taylor L. A. and Neal C. R. (1992) A chemical-model for generating the sources of mare basalts - combined equilibrium and fractional crystallization of the lunar magma-sphere. *Geochim. Cosmochim. Acta* **56**, 3809–3823.

Sossi P. A., Burnham A. D., Badro J., Lanzirotti A., Newville M. and O'Neill H. S. (2020) Redox state of Earth's magma ocean and its Venus-like early atmosphere. *Sci. Adv.* **6**, eabd138710.

Stagno V., Ojwang D. O., McCammon C. A. and Frost D. J. (2013) The oxidation state of the mantle and the extraction of carbon from Earth's interior. *Nature* **493**, 84–88.

Stähler S. C., Khan A., Banerdt W. B., Lognonné P., Giardini D., Ceylan S., Drilleau M., Duran A. C., Garcia R. F., Huang Q. and Kim D. (2021) Seismic detection of the martian core. *Science* **373**, 443–448.

Steenstra E. S., Lin Y., Rai N., Jansen M. and van Westrenen W. (2017) Carbon as the dominant light element in the lunar core. *Am. Mineral.* **102**, 92–97.

Steenstra E. S., Seegers A. X., Putter R., Berndt J., Klemme S., Matveev S., Bullock E. S. and van Westrenen W. (2020) Metal-silicate partitioning systematics of siderophile elements at reducing conditions: A new experimental database. *Icarus* **335**, 113391.

Sundman B. (1991) An assessment of the Fe-O system. *J. Phase Equilibria* **12**, 127–140.

Sutton S., Alexander C. M. O. D., Bryant A., Lanzirotti A., Newville M. and Cloutis E. A. (2017) The bulk valence state of Fe and the origin of water in chondrites. *Geochim. Cosmochim. Acta* **211**, 115–132.

Tait K. T. and Day J. M. D. (2018) Chondritic late accretion to Mars and the nature of shergottite reservoirs. *Earth Planet. Sci. Lett.* **494**, 99–108.

Tarragó M., Le Losq C., Robine T., Reguer S., Thiaudière D. and Neuville D. R. (2022) Redox-induced crystallisation in Ti-bearing glass-forming melts: A Ti K-edge XANES study. *Mater. Lett.* **319**, 132296.

Taylor G. J. (2013) The bulk composition of Mars. *Chemie Der Erde-Geochem.* **73**, 401–420.

Taylor S. R. (1982). *Planetary Science: A Lunar Perspective*. Lunar and Planetary Institute.

Terasaki H., Frost D. J., Rubie D. C. and Langenhorst F. (2007) Interconnectivity of Fe-O-S liquid in polycrystalline silicate perovskite at lower mantle conditions. *Phys. Earth Planet. Inter.* **161**, 170–176.

Trail D., Watson E. B. and Tailby N. D. (2011) The oxidation state of Hadean magmas and implications for early Earth's atmosphere. *Nature* **480**, 79–83.

Usui T., Alexander C. M. O. D., Wang J., Simon J. I. and Jones J. H. (2015) Meteoritic evidence for a previously unrecognized hydrogen reservoir on Mars. *Earth Planet. Sci. Lett.* **410**, 140–151.

Wade J. and Wood B. J. (2005) Core formation and the oxidation state of the Earth. *Earth Planet. Sci. Lett.* **236**, 78–95.

Walker R. J. (2009) Highly siderophile elements in the Earth, Moon and Mars: Update and implications for planetary accretion and differentiation. *Chemie Der Erde-Geochem.* **69**, 101–125.

Wänke H. and Dreibus G. (1994) Chemistry and accretion history of Mars. *Phil. Trans. Roy. Soc. A* **349**, 285–293.

Witt-Eickschen G. and O'Neill H. S. (2005) The effect of temperature on the equilibrium distribution of trace elements between clinopyroxene, orthopyroxene, olivine and spinel in upper mantle peridotite. *Chem. Geol.* **221**, 65–101.

Woodland A. B., Kornprobst J. and Tabit A. (2006) Ferric iron in orogenic lherzolite massifs and controls of oxygen fugacity in the upper mantle. *Lithos* **89**, 222–241.

Wriedt H. A. (1991) The Fe-O (Iron-Oxygen) system. *J. Phase Equilibria* **12**, 170–200.

Yoshizaki T. and McDonough W. F. (2020) The composition of Mars. *Geochim. Cosmochim. Acta* **273**, 137–162.

Zhang H. L., Cottrell E., Solheid P. A., Kelley K. A. and Hirschmann M. M. (2018) Determination of Fe^{3+}/Sigma Fe of XANES basaltic glass standards by Mössbauer spectroscopy and its application to the oxidation state of iron in MORB. *Chem. Geol.* **479**, 166–175.

Zhang H. L., Hirschmann M. M., Cottrell E., Newville M. and Lanzirotti A. (2016) Structural environment of iron and accurate determination of Fe^{3+}/Sigma Fe ratios in andesitic glasses by XANES and Mössbauer spectroscopy. *Chem. Geol.* **428**, 48–58.

Zhang H. L., Hirschmann M. M., Cottrell E. and Withers A. C. (2017) Effect of pressure on Fe^{3+}/SigmaFe ratio in a mafic magma and consequences for magma ocean redox gradients. *Geochim. Cosmochim. Acta* **204**, 83–103.

Associate editor: Wim van Westrenen